FlatChem 57 (2026) 101041

Contents lists available at ScienceDirect

FlatChem

journal homepage: www.sciencedirect.com/journal/flatchem

2D materials as advanced textile finishing for healthcare applications: A comprehensive review

Rim Ben Debabis [a], Agnese D'Agostino [a], Mariam Hadhri [a], Veronica Migani [a], Raphael Palucci Rosa [a], Giuseppe Rosace [a,b], Valentina Trovato [a,b,*]

[a] Department of Engineering and Applied Sciences, University of Bergamo, viale Marconi 5, 24044 Dalmine, BG, Italy
[b] Local CSGI (Inter-University Centre for Colloid and Surface Science) Research Unit, 24044 Dalmine, BG, Italy

ARTICLE INFO

Keywords:
2D materials
Inorganic materials
Smart textiles
Wearable sensors
Healthcare

ABSTRACT

Following the isolation of graphene in the early twenty-first century, research on two-dimensional (2D) materials expanded rapidly, establishing a broad platform for chemistry-driven device innovation. These atomically thin systems, with exceptionally high surface-to-volume ratios, exhibit distinctive chemical, physical, and mechanical responses that are directly relevant to healthcare technologies. Their integration into smart textiles offers a promising route towards unobtrusive, continuous physiological monitoring and personalised interventions informed by real-time data analytics.

This review systematically examines recent and representative applications of 2D materials in health-oriented smart textiles. First, the intrinsic properties that make these materials suitable for wearable health devices are outlined, followed by the analysis of the structural characteristics and transduction mechanisms relevant to textile embodiments. Particular focus is placed on methods for integrating sensors and electronics into everyday clothing, enabling early detection of health issues with minimal disruption to daily routines. The review also assesses current challenges, including the scalability of synthesis, long-term durability, biocompatibility, and regulatory acceptance, and outlines future research directions to facilitate the clinical adoption of this technology.

1. Introduction to the role of smart textiles in advancing healthcare

Chronic and age-related conditions are increasing worldwide and are in dire need of longitudinal measurements beyond clinical settings [1]. Because of that, wearable platforms capable of operating in daily life with minimal user intervention are gaining popularity and attention. For healthcare wearables, the substrate is required to maintain stable signal quality while remaining breathable and comfortable during prolonged skin contact. It must also withstand exposure to sweat, cyclic deformation, and laundering [1,2]. Conventional polymer films and rigid device substrates often struggle to simultaneously provide conformability, breathability, and durability at the garment level. By contrast, textiles are intrinsically porous, drapable, and washable, making them a natural host for continuous monitoring and therapy delivery, provided that functional elements can be integrated without compromising hand feel and wearability [1].

In the present review, the term "smart textiles" is used in line with standard definitions that distinguish predefined functional finishes from textiles exhibiting stimulus–response behaviour enabled by integrated sensing and/or actuation. For healthcare implementations, the dominant integration route is surface finishing, via coating, printing, or fibre/yarn modification, because it enables added functionality while preserving textile mechanics [1,3].

This review focuses specifically on two-dimensional (2D) materials as textile-finishing platforms for healthcare, applied to yarns and fabrics to enable biosignal acquisition (ECG/EMG/EEG), biomechanical and biochemical sensing, thermotherapy/photothermal management, wound care, and antimicrobial protection. Existing reviews have provided valuable overviews of: (i) healthcare e-textile systems at the platform level [1] and (ii) 2D materials for smart textiles more broadly [3], including MXene-enabled smart-textile interfaces [4]. In contrast, the present review places primary emphasis on: (i) fibre–2D material interfacial chemistry and adhesion, (ii) finishing-process compatibility

* Corresponding author at: Department of Engineering and Applied Sciences, University of Bergamo, viale Marconi 5, 24044 Dalmine, BG, Italy.
E-mail address: valentina.trovato@unibg.it (V. Trovato).

https://doi.org/10.1016/j.flatc.2026.101041
Received 19 December 2025; Received in revised form 30 March 2026; Accepted 8 April 2026
Available online 9 April 2026

and wash/mechanical durability, (iii) skin-contact performance (breathability, irritation risk, and skin–electrode impedance stability), and (iv) the way in which these interfacial and process choices translate into healthcare-relevant metrics (e.g., signal-to-noise for biopotentials, gauge factor and hysteresis for strain sensing, stability of skin–electrode impedance, and wash durability) (Fig. 1). Collectively, these considerations define the application-driven trade-offs that guide 2D-material selection for specific healthcare functions [1,3].

Within the broader toolbox of finishing materials (conductive polymers, metal/oxide nanostructures, hydrogels, and hybrids), 2D materials have been repeatedly highlighted as particularly attractive for e-textiles due to (i) high in-plane electrical and thermal transport, (ii) large accessible surface area for mechano-chemo-transduction, and (iii) chemically addressable surfaces/terminations that govern dispersion, fibre adhesion, and stability [3,4]. These attributes are pivotal for constructing percolated networks at low add-on, tailoring skin–electrode interfaces, and coupling textiles to physiological stimuli [3,4]. According to this definition, electronic textiles [1] represent a major subset of smart textiles, integrating elements such as conductive fibres, graphene coatings, and printed metallic traces. When used solely for signal acquisition, these constructs act as passive systems. Adding stretchable batteries, electrochromic layers, or thin-film heaters upgrades them to active systems, and embedding low-power microcontrollers, edge AI processors, and wireless transceivers (such as Bluetooth or NFC) transforms them into ultra-smart platforms [5–9]. Importantly, these enhancements are implemented without compromising drape, breathability, or washability, attributes essential for prolonged wear.

Healthcare-oriented e-textile systems combine textile-native transducers (e.g., dry bioelectrodes; resistive/triboelectric/piezoresistive sensors; conductive yarns) with miniaturised electronics for signal conditioning, embedded processing, wireless communication, and power management. System architectures are most successful when they preserve drape and air permeability while maintaining stable skin–textile contact during motion and after laundering. Reliability is therefore increasingly assessed via defined wear and washing protocols, rather than by single-point laboratory measurements [1].

The global demographic shift towards aging presents substantial opportunities for smart textiles in healthcare, as individuals increasingly pursue proactive self-care. Increased mobile connectivity (5G) and edge AI platforms are further lowering the barriers to adopting these technologies in home health environments [10,11]. The other key sectors include personal protective equipment, defence, sports/leisure, and fashion, as shown in Fig. 2 [6,12,13].

Within healthcare, e-textile platforms can be grouped into monitoring systems (e.g., ECG and movement/respiration sensing using textile electrodes and fibre/yarn transducers) and therapeutic/protective systems (e.g., phototherapy/photothermal textiles, thermal/compression therapy, and wound-care interfaces). This categorisation clarifies which metrics should be prioritised: signal stability and motion-artefact resilience for monitoring, versus dose/temperature homogeneity and safety for therapy. The same distinction is used to structure Sections 3–4 and to define the comparative tables [1,3].

Smart textiles that combine ECG electrodes, Bluetooth® transmitters, and cloud connectivity enable out-of-clinic monitoring with minimal user intervention, provided that signal quality, skin compatibility, and data security are maintained over extended wear [14,15].

However, laundering durability is highly dependent on substrate, binder/encapsulation chemistry, and the wash test programme, and it varies widely across reports. Machine-washable graphene e-textiles produced by scalable pad–dry–cure approaches have been reported to retain high conductivity after home-laundry cycles when suitable compression/encapsulation strategies are used [16]. Polymer-protected MXene-coated cotton has been reported to remain electroconductive even after 20 laundering cycles under defined conditions, highlighting the critical role of protective topcoats in suppressing wash-off and oxidation [17].

These advances support the transition from lab prototypes to user-ready systems compatible with the Internet of Things (IoT) for ongoing out-of-clinic monitoring.

The field of healthcare-oriented smart textiles is characterised by surface-finishing treatments that enable sensing, therapeutic, or protective functions without compromising the wearability of the textiles. In this framework, it is useful to distinguish the principal categories of surface finishing treatments that are most frequently applied to confer such capabilities to textile substrates:

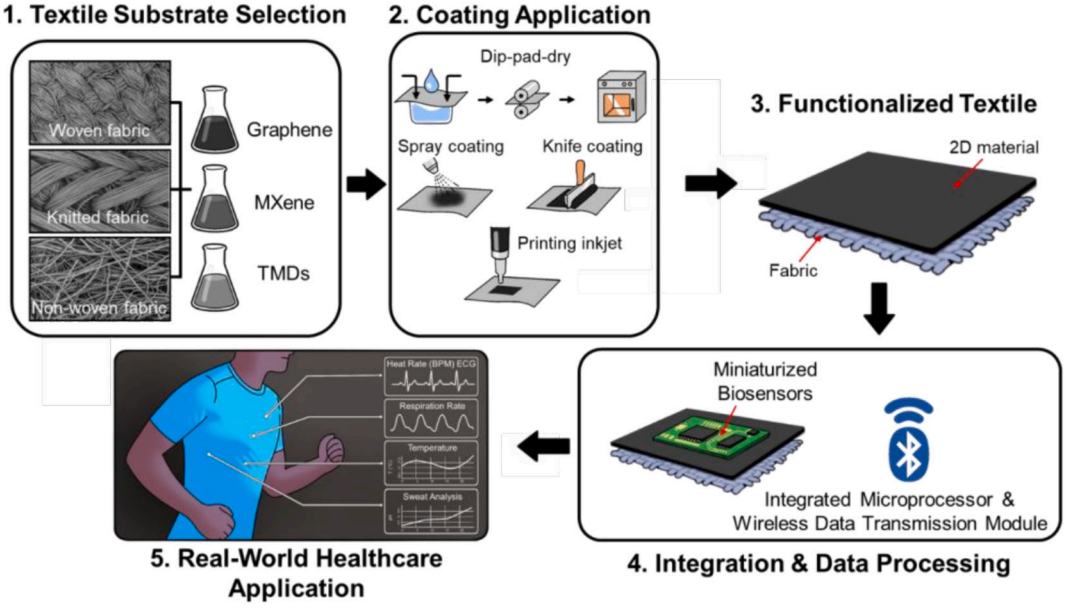

Fig. 1. Conceptual framework for 2D-material-enabled healthcare textiles. The schematic links (1) textile substrate selection and 2D-material ink/coating formulation (e.g.: graphene, MXene, transition metal dichalcogenides (TMDs)), (2) finishing route (dip–pad–dry, spray/knife coating, printing inkjet), (3) interfacial deposition, to (4) integration and data processing and (5) healthcare applications (e.g.: heart/respiration rate, temperature control and sweat analysis). Concepts consolidated from representative e-textile and 2D-smart-textile literature [1,3,4].

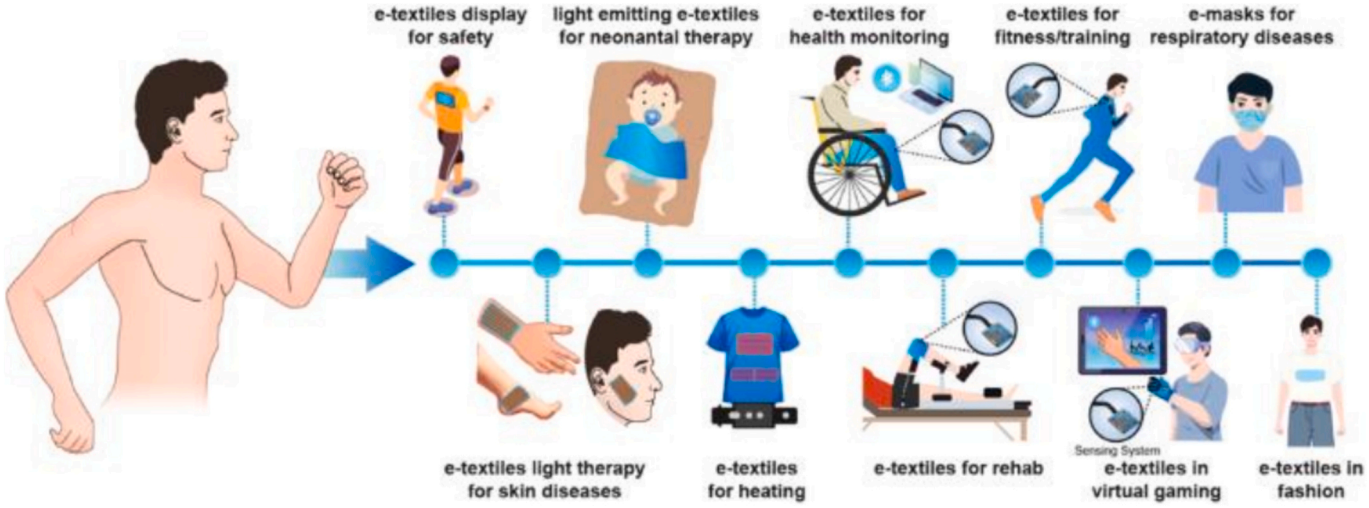

Fig. 2. Schematic illustration of a pathway for e-textile applications across various fields. Reprinted with permission [13].

- **Metal nanoparticles** (Ag, Cu) for antimicrobial effects [18] and electrical conductivity [19];
- **Metal-oxide nanofilms** (ZnO, TiO_2) for UV protection, piezoelectric sensing, and photocatalytic sterilization [20,21];
- **Conductive polymers** (PEDOT:PSS, polyaniline) for flexible electrophysiology [22];
- **Carbon nanostructures** (carbon nanotubes, nanodiamonds) for strain sensitivity and heat regulation [23];
- **Hybrid coatings** (metal–organic frameworks, hydrogels, phase-change microcapsules) for controlled drug delivery or temperature regulation [24,25].

At the nanoscale, reduced dimensionality increases accessible surface area at low mass loading, thereby amplifying interfacial phenomena that govern transduction in wearable textiles. Atomically thin 2D coatings can conform to fibres while preserving textile drape and air permeability, enabling functional finishes that are compatible with garment-level comfort constraints. The practical relevance of 2D materials in healthcare textiles thus depends less on general "material superiority" and more on finish-specific factors, such as ink/coating processability, fibre adhesion, stability under sweat or humidity, resistance to fatigue and laundering, and the stability of the skin-contact interface (especially for bioelectrodes). This review explores these constraints in the next sections [1,3,4].

These attributes have enabled textile-integrated demonstrations in which 2D coatings operate as functional finishes rather than as standalone materials. For example, graphene-based textile ECG electrodes have been reported to yield biosignals comparable to conventional gel electrodes under controlled conditions, including high correlation in textile-printed implementations [26,27]. In MXene-coated or MXene-ink textile sensors, high conductivity allows operation at low driving voltages/currents in resistive sensing geometries, while durability depends strongly on oxidation control and interfacial stabilisation [17].

Therefore, this review synthesises the latest advancements and identifies the research priorities and overarching strategies required to accelerate progress. These textiles must meet strict performance, reliability, and safety standards for deployment in healthcare, reflecting progress from fundamental material research to the integration of smart textile systems.

2. 2D material families and chemistry relevant to healthcare textile finishing

Two-dimensional (2D) materials consist of atomically thin crystals with strong in-plane covalent bonding and weak out-of-plane van der Waals (vdW) interactions. This anisotropy enables exfoliation of the monolayer limits and the stacking of vdW heterostructures without conventional lattice-matching constraints [28]. For wearable healthcare, Å-scale thickness, high specific surface area, and chemically addressable surfaces favour intimate fibre interfaces, efficient transduction, and, when appropriately engineered, improved selectivity to target analytes [29,30].

Although 2D materials are often classified by crystal structure and electronic band character, for healthcare textile finishing, the most practical taxonomy is governed by surface chemistry and environmental stability [3,31]. The key descriptors are: (i) conductivity (and its evolution upon hydration/oxidation) [4,32], (ii) functional groups or surface terminations that control aqueous/solvent dispersibility and enable hydrogen bonding or covalent coupling to common fibres (cellulosics, polyamides, polyesters) [3,4,31], (iii) the propensity to form stable percolated networks on fibrous substrates rather than restacking into brittle films [3,4], and (iv) stability under sweat constituents, detergents, mechanical fatigue, and laundering [1,3]. In the following sections, major 2D families are therefore summarised by highlighting the chemical features that determine (a) processability into textile-compatible coatings/inks and (b) fitness for specific healthcare functions (bioelectrodes, mechanical/biochemical sensing, thermal management, wound care, and antimicrobial barriers) [1,3,4].

Nevertheless, detailed treatments of electronic band structure, growth science (e.g., CVD), and solid-state doping/intercalation are widely available elsewhere and are therefore kept concise here [28,33,34].

The most used 2D materials are summarised below:

- Graphene/Graphene oxide (GO): features a robust sp^2 carbon network with high carrier mobility and chemical tolerance; oxygenated groups in GO (carboxyl, epoxide, hydroxyl) enable covalent/noncovalent coupling that improves dispersion, functionalisation, and adhesion to fibres [35,36];
- Black phosphorus (BP): exhibits directional P—P covalent bonding and a thickness-dependent direct bandgap; surface lone pairs drive ambient reactivity, motivating passivation/encapsulation strategies that affect dispersion stability and interfacial coupling on textiles [37];
- Transition-metal dichalcogenides (TMDs): layered M–X bonding with 2H/1 T/1 T′ polymorphism and strong spin–orbit coupling; chalcogen vacancies and phase control provide surface/reactivity handles that can be leveraged for solution processing,

functionalisation, and fibre adhesion, alongside excitonic/valley effects in 2H monolayers [31,38];

- MXenes: 2D carbides/nitrides with the general formula $M_{n+1}X_nT_x$, where $n = 1–3$ and T_x represent surface terminations (–O/–OH/–F, sometimes —Cl). The latter dictates electronic character, hydrophilicity, redox behaviour and adhesion; hydrophilic terminations support aqueous inks, ion intercalation and strong fabric binding for heating, EMI shielding and sensing [4,39]
- Hexagonal boron nitride (h-BN): a chemically robust, wide-bandgap 2D insulator that provides atomically flat dielectric and barrier layers; functionalisation is accessible primarily at defect and edge sites and at interfaces, influencing multilayer encapsulation and adhesion within textile stacks [35,36];
- Nanostructured carbon nitrides (CNs): sp^2 C—N (tri-*s*-triazine) networks with tunable band gaps and catalytic sites; heteroatom doping and controlled defect formation modulate surface chemistry, dispersion, and coupling to polymer binders/fibres for photocatalytic/antimicrobial or sensing functions [40].

Graphene and graphene oxide provide extended π–π frameworks, together with oxygenated functionalities (carboxyl, epoxide, hydroxyl) that support both covalent and noncovalent grafting to fibres and polymer binders, promoting durable electrical pathways and bio-interfaces on fabrics [34,35]. MXenes exhibit hydrophilic terminations (–O/–OH/–F) inherited from top-down synthesis; these groups enable aqueous processing into stable inks, accommodate ion intercalation, and foster strong interactions with cellulose- and protein-based fibres, providing advantages for Joule heating, EMI shielding, and electrochemical transduction on garments [4]. In contrast, h-BN is chemically resilient and electrically insulating, yet defects and edge sites can be leveraged for functionalisation or used as dielectric/barrier layers within multilayer textile architectures [35]. Collectively, these chemistries underpin stable colloidal dispersions, controlled anchoring to yarns and fabrics, and post-deposition reactivity or passivation capabilities, which are required for wash-durable, skin-compatible healthcare textiles [3,4]. Since their lateral dimensions remain micrometre-scale, 2D nanosheets conform readily to curved or stretchable substrates, an attribute that is beneficial for flexible and wearable sensing applications [3,4,28]. A key design principle is band structure tunability, which is achieved by controlling layer number, stacking/twist, strain, alloying, substitutional doping, intercalation, and the dielectric environment. These levers permit precise adjustment of quasiparticle and optical gaps, band alignment, and interlayer coupling, including interlayer excitons and tunnelling in vdW heterostructures, capabilities that are difficult to access in conventional heteroepitaxy [36,38].

From a textile-finishing perspective, scalable liquid-phase routes are the most relevant, in which exfoliated or chemically derived nanosheets are dispersed in water/solvent formulations using surfactants, polymers, and/or binders, and subsequently immobilised on fibres by drying/curing, in situ polymerisation, crosslinking, or multilayer (e.g., layer-by-layer) assembly [3,4]. Property tuning is commonly implemented through chemistry that directly impacts textile-level performance, including controlling oxidation state and functional-group density (e.g., GO reduction), tailoring surface termination chemistry (e.g., MXene T_x groups), and noncovalent/covalent grafting of polymers or biomolecules to enhance fibre adhesion, mitigate degradation pathways, and stabilise the skin-contact interface [1,4,31].

Three main strategies are used: (i) substitutional doping, which involves incorporating heteroatoms into the lattice via CVD/CVT growth, electrochemical or thermal substitution, hydrothermal routes, or ion exchange; (ii) intercalation, involving the insertion of atoms, ions, or molecules into vdW gaps using liquid, electrochemical, or solvent-free methods; and (iii) surface functionalisation, involving charge-transfer or covalent chemistry at basal diffusion planes or edges that minimises bulk diffusion. These approaches enable control over carrier density and Fermi-level position, which can influence excitonic dynamics and, where demonstrated, magnetic responses. They also support band-structure engineering in vdW heterostructures [38]. However, trade-offs related to uniformity, reversibility, defect generation, and environmental stability should be clearly evaluated [31]. Beyond chemical modification, control of the dielectric environment and encapsulation are equally decisive for device performance. Given the high surface-to-volume ratio in two dimensions, interfacial dielectrics and passivation layers strongly influence charge scattering, phonon coupling, and stability. Black phosphorus exemplifies these issues: photo-assisted oxidation and ambient degradation can be mitigated by atomic layer deposition (ALD) or full encapsulation, establishing a model case for managing air-sensitive 2D semiconductors [37]. Encapsulation with hexagonal boron nitride (h-BN) reduces charged-impurity scattering and remote phonon coupling, allowing devices to approach intrinsic performance limits [36]. Advances in characterisation, including Raman and photoluminescence spectroscopy, angle-resolved photoemission spectroscopy (ARPES), cathodoluminescence, scanning probe microscopy, and high-resolution TEM, now enable correlations between atomic-scale chemistry and macroscopic device performance [41]. Such multimodal metrology is essential for process optimisation, where low disorder and clean interfaces are critical [35]. Device-level studies have further clarified how contact geometry, phase-engineered contacts, and dielectric choice mitigate Schottky barriers, hysteresis, and electrical noise, translating chemical control into circuit-relevant improvements [36]. Despite substantial progress, several chemically rooted challenges remain. First, synthesis must achieve atomic-scale uniformity in composition, phase, and defect density over large areas, including controllable alloying and sharply defined lateral/vertical heterojunctions [28]. Second, operational stability under realistic environments requires effective passivation chemistries and benign encapsulants that are compatible with flexible substrates [37]. Third, defect and dopant metrology must resolve spatial inhomogeneity arising from certain doping and intercalation routes to ensure reproducible, high-yield fabrication [31]. Integration approaches, ranging from direct growth of 2D materials to transfer methods that minimize contamination, must be further optimised to achieve high throughput and reliability, supporting the large-scale adoption of 2D heterostructures in electronic and optoelectronic technologies [36]. The following subsections provide a detailed exploration of specific families of 2D materials, including graphene, black phosphorus, transition-metal dichalcogenides, MXenes, hexagonal boron nitride, and carbon nitrides, highlighting their synthesis, intrinsic properties, and potential applications in textile integration for biomedical monitoring [3].

2.1. Graphene

Graphene and its derivatives (graphene nanoplatelets, graphene inks, graphene oxide (GO) and reduced GO) are among the most widely adopted 2D materials in healthcare textiles because they can form mechanically compliant, electrically percolated networks on fibrous substrates at low add-on while remaining compatible with scalable liquid-phase finishing (padding/coating/printing) [1,3]. There are many works in the literature that discuss in great detail the graphene band structure and the film quality [28,34]. Instead, in this review, emphasis is placed on the parameters that govern textile performance and translation, including dispersibility, fibre adhesion (binder/crosslinking strategies), crack tolerance under cyclic deformation, and retention of conductivity/signal quality after sweat exposure and laundering [1,3].

For textile finishing, the most relevant graphene routes are those enabling stable liquid-phase formulations (e.g., graphene nanoplatelets, graphene inks, GO and reduced-GO dispersions) compatible with coating, padding, and printing [3]. While CVD growth can yield high-quality continuous films for electronics, such approaches are generally less consistent with scalable garment finishing than solution-processed coatings that can be immobilised using binders, crosslinking, and encapsulation strategies tailored to wash durability and mechanical

fatigue resistance [1,3].

Chemical modification. The delocalised π-electron system of graphene enables both covalent and noncovalent approaches to tune its electronic structure. Covalent functionalisation, such as radical addition or diazonium-based reactions and grafting at lattice vacancies, locally converts sp^2 carbon to sp^3, thereby opening transport gaps or creating robust anchoring sites. While these modifications expand graphene's capabilities for sensing and interfacial applications, they also introduce additional scattering centres, necessitating careful quantification of mobility–noise trade-offs [35]. Noncovalent modification strategies, including charge-transfer doping, π–π stacking interactions, and coordination with molecular adsorbates, shift the Fermi level without significant lattice disruption. However, issues such as dopant desorption and temporal drift motivate the use of encapsulation strategies and in situ metrology for stability assessment [31]. Intercalation, whether between graphene and its supporting substrate or between layers in multilayer graphene stacks, provides reversible control over carrier density and screening effects, complementing electrostatic gating in device architectures [31].

Outlook. For healthcare textiles, the most impactful graphene-related research directions concern formulation and interface engineering rather than incremental advances in film-quality growth: robust ink/coating chemistries, scalable immobilisation routes on diverse fibres, and protective architectures that preserve breathability while improving fatigue and laundering durability [1,3].

2.2. Black phosphorus

The isolation of phosphorene, the monolayer form of black phosphorus (BP), via mechanical exfoliation in 2014 [28], catalysed the rapid expansion of research on this anisotropic 2D material. Like other layered materials, BP consists of sheets held together by van der Waals forces, allowing exfoliation methods similar to those for graphene (Fig. 3) [3]. Unlike graphene's planar sp^2 bonding, BP adopts sp^3 hybridisation in a puckered lattice with a buckled armchair direction and a bilayer zigzag configuration [42]. Each phosphorus atom forms three covalent bonds, two in-plane and one out-of-plane, with slightly shorter P—P distances within a layer than across layers; the characteristic bond angles are 96.16° (in-plane) and 102.42° (out-of-plane) [42,43].

This anisotropic lattice gives rise to pronounced in-plane anisotropy in electrical, optical, and mechanical properties [44,45].

BP's band gap is thickness-dependent, ranging from ~1.5 eV (monolayer) to ~0.3 eV (bulk), and its hole mobility can exceed 1000 $cm^2\ V^{-1}\ s^{-1}$ [46]. However, BP is chemically unstable under ambient oxygen, moisture, and light, undergoing rapid photooxidation. Passivation strategies include encapsulation with h-BN, polymer coatings, or thin oxides, although such barriers may compromise sensing effectiveness [37]. Large-scale synthesis is currently hindered by cost, complex reaction conditions, and safety concerns due to the reactivity, toxicity, and flammability of BP.

Chemical modification. Chemical modification offers pathways to enhance BP's stability, tailor its electronic properties, and broaden its range of applications. Covalent functionalisation, such as aryl diazonium chemistry, reacts preferentially at defect and edge sites, enabling passivation while modulating conductivity [47]. Noncovalent strategies, such as charge-transfer dopants, surfactants, or molecular adsorption, offer tunability with minimal lattice disruption. However, dopant desorption and instability necessitate encapsulation for long-term use [31,48]. Intercalation of small molecules or metal ions between BP layers can adjust interlayer spacing, alter the band gap, and modify transport properties without bulk substitution [37].

Functional composites represent another route to enhancing stability and diversifying performance. Li et al. developed a multifunctional cotton fabric for electromagnetic interference (EMI) shielding and fire safety by blade-coating phosphorene/MXene ($Ti_3C_2T_x$)/sodium alginate inks, followed by polydimethylsiloxane treatment to improve wash durability [49]. The effectiveness of EMI shielding was tunable between 17 and 53 dB by adjusting the coating density, with hydrophobicity up to 125.9° and rapid thermal recovery within 10 s. Increasing the coating weight reduced both the peak and total heat release, attributed to $Ti_3C_2T_x$ forming a conductive 3D network [49].

Outlook. For BP-enabled textiles, environmental stability is the dominant translation barrier; encapsulation and passivation strategies must be compatible with flexible, breathable substrates and withstand sweat/humidity and laundering. Accordingly, finishing architectures that preserve function while limiting ambient degradation should be prioritised over extended fundamental growth narratives within a textile-focused review [1,37].

2.3. Transition-metal dichalcogenides (TMDs)

Transition-metal dichalcogenides (TMDs) are compounds of the general formula MX_2, where M is a transition metal and X is a chalcogen [31]. Representative examples include MoS_2, VS_2, WS_2, and WSe_2, which exhibit wide band gaps (> 1 eV) alongside favourable electrical and mechanical properties, making them highly relevant for wearable sensing applications [50]. In particular, monolayer MoS_2 nanosheets combine high flexibility with biocompatibility, and TMD-based composites can enhance quantum yield, selectivity, and sensitivity in flexible sensors [51].

In the bulk state, TMDs are formed by layers of transition-metal atoms sandwiched between two layers of chalcogen atoms, with six chalcogen atoms coordinating each metal atom. These layers are bound by van der Waals forces, enabling mechanical or chemical exfoliation. MoS_2 exists in several polymorphs, including the thermodynamically stable 2H phase and the metastable 1 T and 3R phases, which can be derived from 2H under suitable chemical or electrochemical conditions [52]. In the 2H phase, the layers adopt trigonal-prismatic coordination (a = 3.15 Å, c = 12.30 Å; space group $P6_3/mmc$) [53].

From a textile-finishing perspective, the primary relevance of TMD synthesis and phase/defect chemistry lies in their effects on

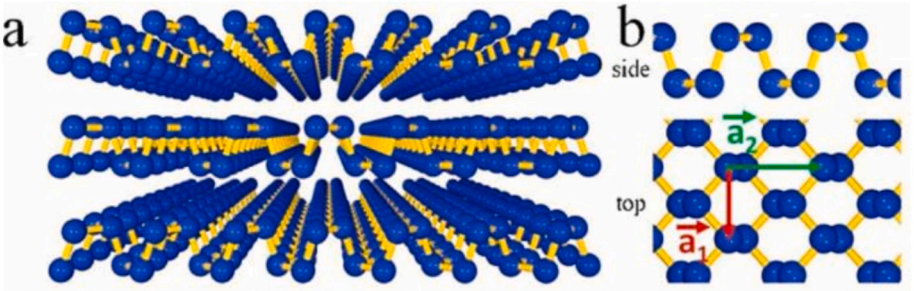

Fig. 3. Crystal and electronic structures of few-layer phosphorene: (a) side-view representation highlighting the layered arrangement and (b) side and top perspectives of few-layer phosphorene. Reprinted with permission [3].

dispersibility, fibre-network formation, and environmental stability under humidity/sweat and repeated deformation [3,37]. Although CVD and intercalation-enabled phase control are central to device-grade films, textile implementations more often depend on coating or printing formulations (frequently as hybrids), where interfacial adhesion, crack tolerance, and wash-off resistance become the main performance factors [1,3].

In healthcare textile finishing, TMDs are primarily applied through solution-processable flakes and hybrid coatings, where their functional performance depends on network formation on fibres, interfacial adhesion, and environmental stability rather than on device-grade films quality [1,3]. While phase and defect engineering, as well as CVD growth, are central to the broader field of TMD electronics, their relevance in textile applications is more often indirect. In healthcare textiles, their importance lies mainly in how they influence dispersibility, conductivity, and resistance to degradation under humidity, sweat exposure, and repeated mechanical deformation [37]. Accordingly, the discussion prioritises textile-compatible processing and the trade-offs most frequently encountered in wearables (signal level versus mechanical robustness; sensitivity versus stability; and performance retention after laundering), rather than providing an exhaustive survey of growth and electronic-structure studies [1,3].

Chemical modification. Heterostructure engineering has been widely applied to TMDs to enhance performance. Park et al. employed laser-beam annealing to selectively grow WS_2 on top of MoS_2, creating a WS_2/MoS_2 heterojunction strain sensor capable of stable wrist-motion monitoring [54]. Lee et al. designed a high-performance strain sensor based on a MoS_2/graphene heterostructure, in which piezoelectric charges in MoS_2 shifted the graphene Fermi level under strain, modulating the Schottky barrier. This approach achieved an exceptionally high gauge factor of 5.8×10^5, approximately 500 times greater than conventional metal/MoS_2 sensors [54].

Outlook. In textile implementations of TMDs, the most impactful advances are expected from coating/printing-compatible formulations and hybrid architectures that deliver stable, repeatable performance under deformation and washing. More information about the topics, such as wafer-scale growth and band-structure optimisation, can be found in the literature [3,28,37].

2.4. Transition-metal carbides/nitrides (MXenes)

Since first being reported on in 2011, transition-metal carbides,

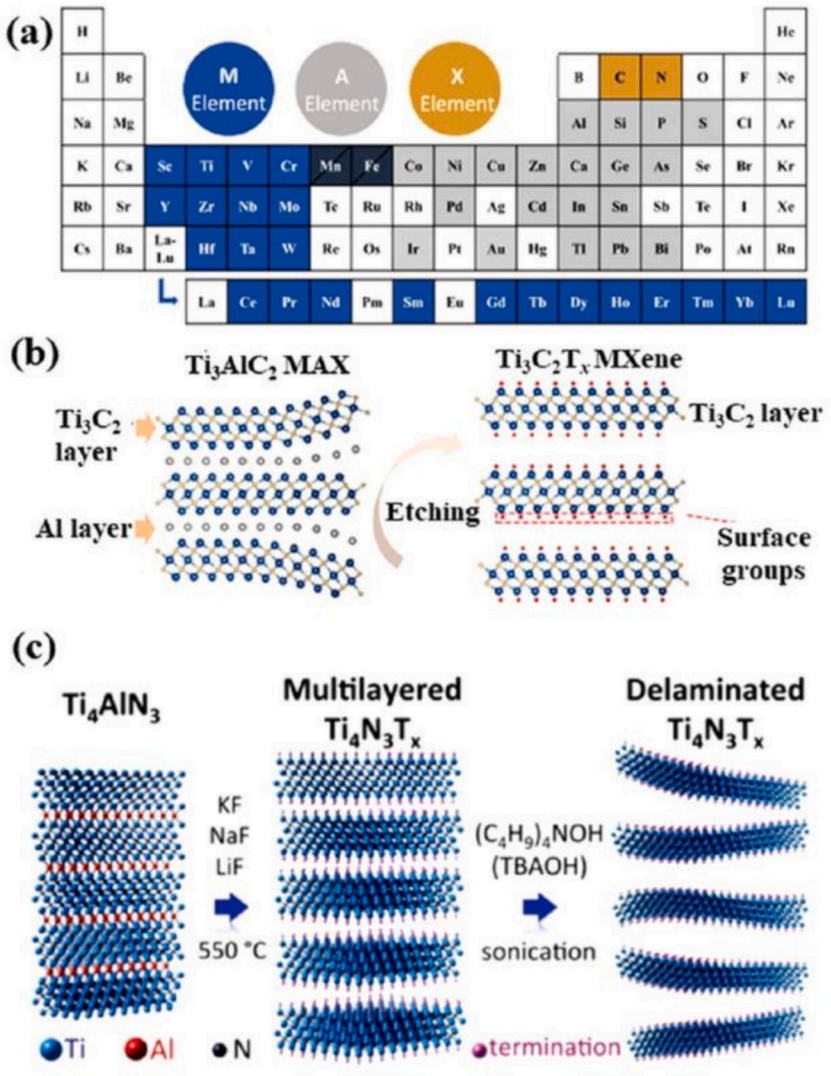

Fig. 4. From MAX phases to MXenes: schematic of selective etching routes and surface terminations (T_x = –O/–OH/–F/–Cl) that govern inkability, hydrophilicity, and electronic behaviour. (a) Periodic table of the elements showing the updated MAX phase compositions, including the recently reported novel MAX phases with A = Co, Ni, Cu, Zn, and so on; Mn and Fe may appear in either the M or A positions. (b) Schematic representation of the selective etching process converting Ti_3AlC_2 MAX phase precursor into $Ti_3C_2T_x$ MXene. Reprinted with permission [4]. (c) Etching with molten salt. Reprinted with permission [58].

nitrides, and carbonitrides, collectively known as MXenes, have emerged as a significant class of 2D materials with promising photocatalytic, electronic, and electrochemical properties [55]. MXenes adopt general formulas $M_{n+1}X_n$ or $M_{n+1}X_nT_x$ (n = 1–3), where M denotes an early transition metal (e.g., Ti, Zr, V, Nb, Mo), X is carbon or nitrogen, and T_x represents surface terminations, such as –OH, —O, or —F [56]. These terminations significantly influence hydrophilicity, conductivity, and electrochemical behaviour. Fig. 4 schematically traces MAX-to-MXene conversion routes and highlights how surface terminations (T_x = –O/–OH/–F/–Cl) govern inkability, hydrophilicity, and interfacial adhesion on fibres [4,57]. Updated MAX phase compositions across the periodic table are presented in Fig. 4a [57]. The schematic of MAX phase exfoliation and MXene formation is shown in Fig. 4b [57], and the alternative moulten salt etching approach is illustrated in Fig. 8c [58].

MXenes exhibit metallic-level conductivity (up to ~10^5 S cm^{-1}), substantial volumetric pseudocapacitance (up to 1600 F cm^{-3}), robust mechanical properties, and excellent dispersibility in aqueous media, making them promising for wearable energy storage, sensing, and flexible electronics [52]. However, achieving simultaneous optimisation of electrical, electrochemical, and mechanical performance remains challenging due to weak interlayer interactions, small flake size, and a tendency to restack [59].

Chemical modification. Surface functionalisation and composite engineering offer effective routes for enhancing MXene performance. Zhang et al. [60] developed a self-healing $Ti_3C_2T_x$ MXene/polydimethylsiloxane (PDMS) supramolecular elastomer, in which hydrogen bonding and dynamic imine linkages enable room-temperature self-healing. The material retained nearly full mechanical integrity and conductivity after damage, with uniform MXene dispersion ensuring high electrical sensitivity for monitoring large-amplitude and subtle muscle motions (Fig. 5a) [60].

Ren et al. [61] demonstrated a highly sensitive MXene–perovskite image sensor array (1250 pixels), where synergistic energy-level alignment and near-infrared resonance between $Ti_3C_2T_x$ and the perovskite absorber produced a responsivity of 84.77 A W^{-1}, detectivity of 3.22 × 10^{12} Jones, and a linear dynamic range up to 82 dB across the visible–NIR spectrum (Fig. 5b, c) [61].

MXene-based composites further expand the range of applications. Chao et al. [62] fabricated a wearable MXene/polyaniline fibre (PANIF) strain sensor on an elastic rubber substrate. This laminated architecture exhibited a low strain detection limit (0.1538%), high sensitivity (gauge factor up to 2369.1), and excellent durability, with reliable detection of human motions up to 80% strain (Fig. 6). Li et al. [63] produced pure $Ti_3C_2T_x$ MXene aerogel fibres via dynamic sol–gel spinning and supercritical CO_2 drying, yielding oriented mesopores and high conductivity for dual electrothermal and photothermal actuation, features attractive for smart textiles and portable devices.

Outlook. For MXene textiles, oxidation and humidity-driven drift frequently limit long-wear reliability, therefore, paying attention to surface chemistry during manufacturing, reducing surface defects, and adding coatings that protect without sealing the material too much are key ways to expand its adoption. Comparative evaluation should prioritise stability retention (sweat/humidity aging, fatigue, laundering) alongside sensitivity and low-voltage operation [1,3,4].

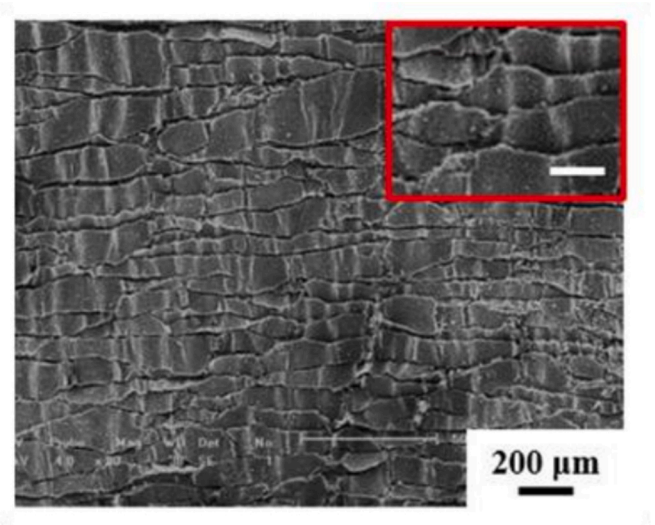

Fig. 6. SEM image of a wearable strain sensor based on MXene nanocomposites with a tile-like stacked hierarchical microstructure. Adapted with permission [62].

2.5. Boron nitride (BN)

As shown in Fig. 7a, hexagonal boron nitride (h-BN) provides an atomically flat dielectric platform. Its diagnostic Raman E2g mode appears near 1366 cm^{-1} in bulk, and blue-shifts by ~4 cm^{-1} in monolayers due to phonon hardening upon removal of interlayer coupling (Fig. 7c). Small red-shifts (~1–2 cm^{-1}) are frequently observed in few-layer samples, reflecting random strain introduced during exfoliation [64]. Thickness identification, often challenging by conventional microscopy, can be aided by monochromatic-light optical contrast (Fig. 7b) and by the decrease of E2g intensity with decreasing thickness, noting that absolute intensities are sensitive to interference and instrumental conditions [64].

In h-BN and r-BN, boron, and nitrogen atoms adopt sp^2 hybridisation, forming layered structures, whereas in c-BN and w-BN, they exhibit sp^3 hybridisation. Differences in stacking sequences along the c-axis result in ABA–BAB or ABC arrangements. Under ambient conditions, h-BN is the most thermodynamically stable phase, while c-BN is notable for its extreme hardness and wear resistance. The weak interlayer forces in h-BN facilitate exfoliation from bulk-layered crystals into

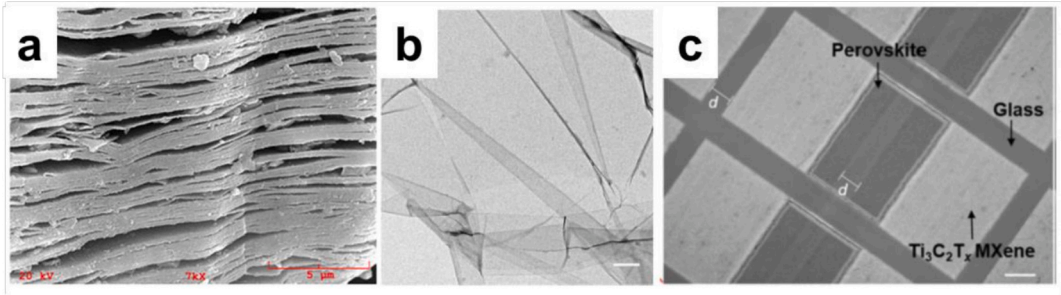

Fig. 5. (a) SEM micrograph of multilayer-stacked $Ti_3C_2T_x$ MXene (A-MXene) sheets, illustrating their characteristic layered structure. Reprinted with permission [60]. (b) Bright-field TEM image of thin $Ti_3C_2T_x$ MXene nanosheets, evidencing their few-layer and transparent morphology (scale bar: 300 nm). (c) Optical image of a single pixel from an MXene–perovskite image sensor array, where $Ti_3C_2T_x$ MXene functions as the electrode and perovskite forms the photoactive layer; the channel width of the MXene electrodes d is 120 µm (scale bar: 200 µm). Reprinted with permission [61].

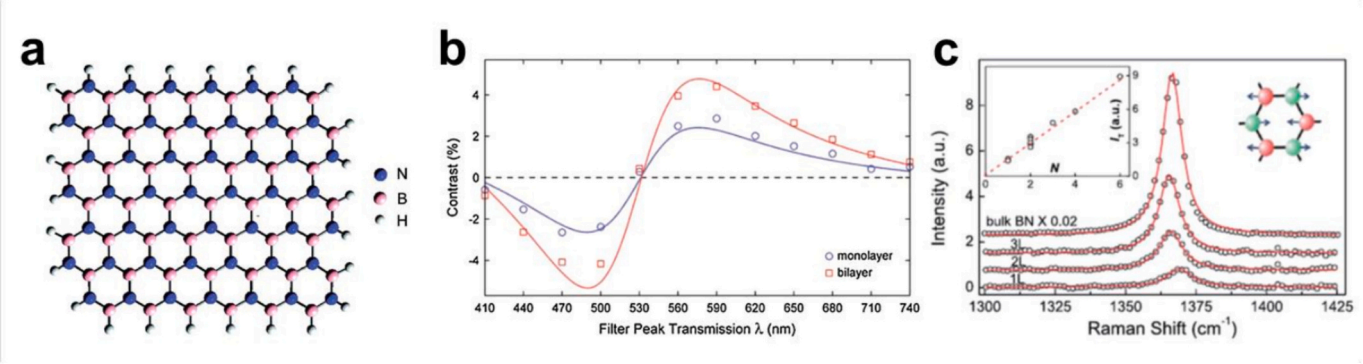

Fig. 7. Hexagonal boron nitride (h-BN): (a) h- BN flat structure diagram (blue on behalf of nitrogen atoms and pink on behalf of boron atoms, respectively) [64]. (b) Difference in optical contrast of mono- and bilayer h-BN with respect to wavelength of light. Reprinted with permission [65]. (c) Raman spectra of 2D h-BN [64]. (For interpretation of the references to colour in this figure legend, the reader is referred to the web version of this article.)

nanosheets, nanoribbons (BNNRs), and multiwall BN nanotubes (MWBNNTs) [42]. Due to its high biocompatibility, wide band gap (~5.9 eV), high thermal conductivity, and large specific surface area, h-BN is an attractive candidate for wearable sensing and optoelectronic applications [50].

Chemical modification. Heterostructuring and surface functionalisation have expanded the applicability of h-BN in flexible electronics. De Souza et al. [66] demonstrated a flexible NO/NO_2 gas sensor based on an h-BN/graphene heterostructure, achieving high selectivity and sensitivity, with stable electronic transport geometry. As shown in Fig. 8a, the device consists of CN and CB interfaces connected by a central graphene channel, while Fig. 8b depicts the most stable adsorption geometries of gas molecules after full relaxation. This performance was attributed to h-BN's atomically smooth, dangling, bond-free surface, which preserves graphene's high carrier mobility while providing chemical robustness.

The pre-oriented h-BN guides the nucleation, alignment, and stress relief of ZnO nanocolumn arrays, yielding highly uniform morphologies (Fig. 9a) [67]. The corresponding schematic (Fig. 9b) illustrates the vertically aligned ZnO nanoarrays grown on the h-BN/Cu paper substrate, highlighting the role of the h-BN layer in directing ZnO growth and ensuring structural uniformity [67].

Incorporating h-BN into a ZnO nanocolumn/h-BN sandwich structure created a flexible, transparent piezoelectric nanogenerator with a monolayer dielectric interface. This device achieved a power-generation density of 169 mW cm^{-2} and successfully harvested mechanical energy from human motion, demonstrating its suitability for powering smart, portable chargers.

Outlook. In healthcare textiles, h-BN is most relevant as a chemically robust dielectric, barrier, and encapsulation/interlayer material that can improve the environmental stability of conductive 2D coatings and mitigate degradation pathways without sacrificing flexibility [3]. Accordingly, for the next step in textile deployment, the research should be focused on large-area, textile-compatible deposition/lamination strategies and interface engineering that preserve breathability while improving wash durability and mechanical fatigue resistance in multilayer stacks [1].

2.6. Nanostructured carbon nitrides (CNs)

Nanostructured carbon nitrides (CNs) encompass a family of polymeric materials derived from nitrogen-rich precursors, with structural diversity arising from their degree of condensation. Linear 'melon-like' polymers consist of *s*-triazine units connected via secondary nitrogen linkages, whereas graphitic carbon nitride (g-C_3N_4) forms stacked 2D sheets of tristriazine units linked by planar tertiary amines. Among these, g-C_3N_4 is generally the most thermodynamically stable, exhibiting high hardness, chemical inertness, and distinctive lamellar morphology [68–70].

The high nitrogen content and intrinsic chemical/thermal stability, combined with a band gap of ~2.7 eV and conduction/valence band

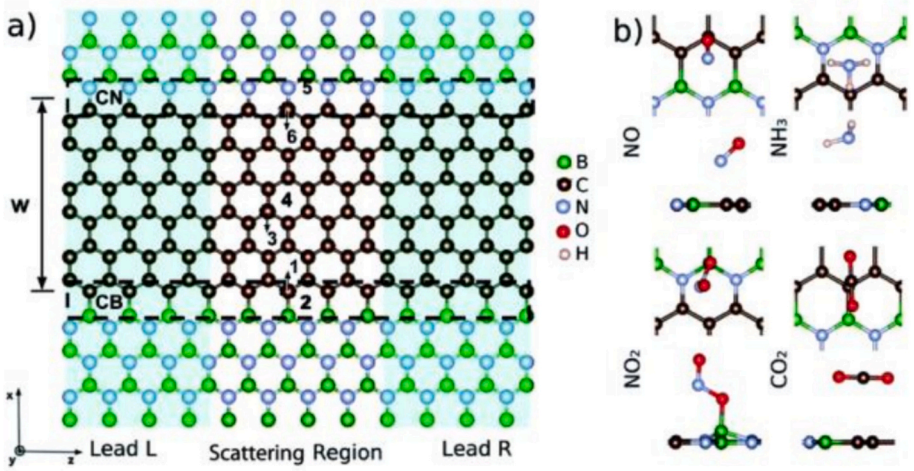

Fig. 8. The G-hBN sensing device corresponds to electronic transport. This chart illustrates the stable geometric structure. (a) Top view of the designed G–hBN sensor within the electronic transport framework, consisting of the scattering region and left/right electrodes. Adsorption sites for gas molecules are labelled 1–6, while the two interface types are marked as CB and CN. (b) Optimised configurations of NO, NO_2, NH_3, and CO_2 on their most favourable adsorption sites, illustrated in both the top and side views. Atom types are distinguished using the colour code provided in the legend [66].

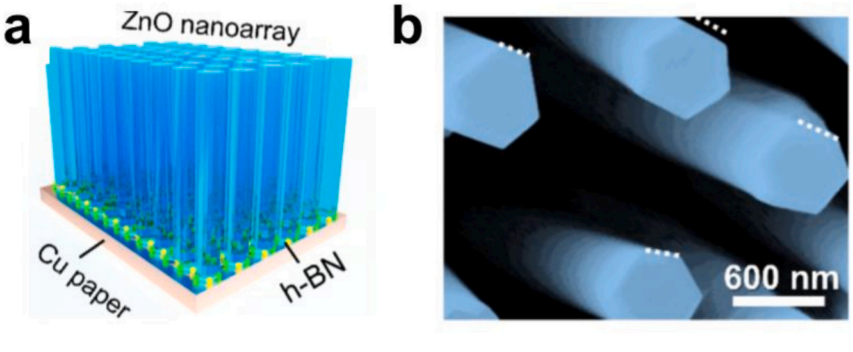

Fig. 9. (a) Magnified SEM image revealing the structural morphology of the ZnO nanoarray. (b) Schematic illustration of vertically aligned ZnO nanoarrays grown on h-BN/Cu paper substrate. Reprinted with permission [67].

positions compatible with visible-light-driven photocatalysis, make g-C_3N_4 attractive for a wide range of applications, including catalysis, hydrogen storage, photocatalysis, biomedical devices, water purification, and energy conversion [71–75]. Its structure is proposed to derive from either condensed *s*-triazine units (with periodic carbon vacancies) or tristriazine subunits (with greater local stability), the latter often being favoured in experimental reports [76]. The most common synthesis method involves pyrolysing inexpensive precursors such as melamine, urea, thiourea, dicyandiamide (DCDA), or cyanamide. Precursor chemistry, heating rate, and pyrolysis temperature significantly affect crystallinity, electronic structure, and band gap [77–79].

Chemical modification. Recent work has expanded the functional scope of g-C_3N_4 in smart textile applications, particularly in energy harvesting and sensing. Bayan et al. [80] developed a triboelectric nanogenerator (TENG) by loading Ag nanoparticles onto g-C_3N_4 nanosheets supported on carbon fibres. An interfacial nylon layer between the triboelectric g-C_3N_4 and the carbon cloth optimised charge separation and improved device output. When paired with Teflon and mechanical agitation, the bi-layer AgCN/nylon TENG produced an open-circuit voltage of ~200 V and charged a commercial capacitor to ~85 V within 30 s. Integrated into garments, it harvested energy from various human motions, including hand, finger, and wrist movements.

In another example, Mohammad et al. [81] fabricated flexible electrodes on carbon cloth modified with spherical Al_2O_3 and Al_2O_3/g-C_3N_4 composites via hydrothermal synthesis for non-enzymatic H_2O_2 detection. Al_2O_3/CC electrodes exhibited a detection limit of 1.1×10^{-4} M and sensitivity of 58 μA mM^{-1} cm^{-2}, whereas Al_2O_3/g-C_3N_4/CC electrodes achieved a detection limit of 1.6×10^{-4} M with significantly higher sensitivity (108 μA mM^{-1} cm^{-2}). Both systems demonstrated excellent reproducibility, repeatability, and stability [81].

Outlook. For CN-based textile finishes, their application depends on immobilisation strategies that prevent wash-off and maintain mechanical integrity, while tailoring functional performance through controlled hybridisation where conductivity is required. Future analysis should therefore focus textile-level durability and exposure-relevant stability in addition to functional demonstrations [3,31].

2.7. Fibre–2D material interfacial chemistry, adhesion, and degradation mechanisms: Textile-finishing perspective

In textile finishing, poor interfacial performance is the most common cause of problems. Fibre chemistry governs initial adhesion and durability: cellulose-based materials provide hydroxyl-rich surfaces that can support hydrogen bonding and electrostatic interactions with oxygenated or terminated 2D surfaces, whereas synthetic fibres (e.g., polyesters) often require surface activation or primer/binder strategies to achieve robust anchoring [3,4]. Practical immobilisation commonly relies on polymeric binders/crosslinkers and multilayer structures that stabilise percolated networks against delamination, cracking, and wash-off, but these approaches can introduce trade-offs in breathability, hand feel, and strain-transfer efficiency [1,3].

Degradation under realistic wear is typically multifactorial: cyclic deformation can drive network fragmentation and interfacial debonding, laundering introduces mechanical abrasion and detergent-mediated extraction, and sweat/humidity can accelerate oxidation or conductivity drift in susceptible 2D systems. These mechanisms explain why "high sensitivity" reported in static tests may not translate into stable garment performance without explicit strategies for interfacial stabilisation and environmental protection [1,3,4].

3. Integration of 2D materials into smart textiles for healthcare applications

This section evaluates strategies for integrating 2D materials into smart textiles, with a focus on healthcare-relevant performance, compatibility with standard textile processing, and durability. Particular emphasis is placed on embedding routes that enable passive diagnostics and the continuous monitoring of vital signs directly on garments [1,3]. Piezoresistive strain sensors are essential for wearables, but conventional designs rarely provide both a wide operating range and high sensitivity. Layered 2D structures can increase gauge factors and detect subtle physiological movements. Techniques such as porosity adjustment, aerogel networks, and micro/meso-patterning further enhance amplitude, linearity, and noise resistance in flexible and textile applications [3,82].

Among 2D materials, graphene and its derivatives have been widely explored in textile formats owing to their high conductivity, chemical stability, and mechanical compliance, enabling conformal strain sensors and bioelectrodes that tolerate repeated deformation and home laundering [16]. Selected transition-metal dichalcogenides (TMDs), such as MoS_2 and WS_2, exhibit semiconducting properties and monolayer piezoelectricity, enabling multifunctional sensing of strain and pressure as well as coupling to mechano-electrical transduction [83]. MXenes (e.g., $Ti_3C_2T_x$) combine near-metallic conductivity with hydrophilicity and surface terminations conducive to stable coatings/inks, delivering textile electrodes, strain/pressure sensors, and energy modules via aqueous processing [4]. Hexagonal boron nitride (h-BN) functions as a chemically robust, electrically insulating interlayer that helps preserve device performance and longevity without sacrificing flexibility [84]. Graphitic carbon nitride (g-C_3N_4) provides a metal-free, photocatalytic platform for light-assisted biosensing and self-cleaning/antimicrobial textile finishes [40]. Leveraging these material attributes, such as conductivity, flexibility, chemical stability, and tunable electronic structure, has enabled the development of textile devices with enhanced sensitivity, faster responses, and improved environmental stability. The following sections analyse fabrication routes, application-specific

architectures, and performance metrics for 2D-enabled textile systems in real-time healthcare monitoring, with an emphasis on wash durability and skin compatibility [1,3].

Using cross-study comparison, the following subsections examine material systems and textile implementations within a common comparative framework. For each healthcare function, performance is discussed using broadly aligned descriptors that capture electrical behaviour, sensing or transduction characteristics, and operational reliability. These include parameters such as sheet resistance and operating voltage/current for active devices; gauge factor and working strain range for motion sensing; skin–electrode impedance and signal-quality surrogates for ECG; response and recovery times, as well as dynamic range, for humidity and respiration sensing; and temperature coefficient and resolution for thermometric applications [1,3].

In addition, key textile-level constraints are treated explicitly across functions, including (i) mechanical fatigue of percolated 2D networks under repeated bending/stretching, (ii) laundering degradation mechanisms (wash-off, abrasion, and chemistry-driven drift), (iii) environmental stability under sweat/humidity, and (iv) interface stability in skin-contact measurements (e.g., bioelectrode contact quality and motion artefacts) [1,3,4].

3.1. Garment-level integration metrics: Fatigue, laundering, and skin–electrode interface stability

For healthcare wearables, textile prototypes should be interpreted using garment-level reliability metrics in addition to headline sensitivity. Mechanical fatigue under repeated deformation can introduce progressive drift via crack growth, network rearrangement, and interfacial debonding, while laundering can cause conductivity loss through wash-off, abrasion, and binder swelling/extraction [1,3].

For biopotential electrodes (e.g., ECG), stable performance is governed not only by electrode conductivity but also by skin-electrode impedance stability, motion artefacts, and comfort during prolonged wear. These factors are influenced by textile compliance, surface roughness, moisture management, and coating architecture, and they motivate the use of interface-stabilising strategies (binder/encapsulation design and contact optimisation) when translating 2D coatings into clinically credible garments [1,2].

3.2. Human physiological activity (body movement) sensors

Across textile strain/pressure sensing, most 2D-material systems operate via piezoresistive percolation networks, so performance is governed as much by network architecture and fibre–coating adhesion as by intrinsic conductivity. Graphene-based finishes generally provide comparatively robust conductivity and chemical stability, supporting wearable strain sensing with favourable wash tolerance when adhesion/encapsulation are appropriately engineered. However, sensitivity often relies on microstructuring (porosity, cracks, hierarchical roughness) rather than intrinsic band effects. MXenes typically enable high signal levels at low operating voltages due to near-metallic conductivity and hydrophilic terminations that favour aqueous processing and strong fibre interactions, but long-term performance can be limited by oxidation and environmental instability if passivation is insufficient. Semiconducting TMDs and black phosphorus can contribute additional transduction pathways (e.g., piezoelectric or semiconducting responses), but practical textile deployment frequently requires hybridisation or interface engineering to offset lower conductivity and, for BP, ambient instability [3,4,37].

Graphene-based fabrics prepared via dip-coating or pad–dry–cure routes yield conformal, high-strain piezoresistive sensors on common textiles. Repeated dip-coating of cotton with graphene, followed by elastomer encapsulation, yields stable devices with high sensitivity and long cycling endurance, making them suitable for tracking joint motion, speech, and heartbeat [85]. On polyester substrates, multifunctional rGO/polyester fabrics combine low sheet resistance with reliable strain sensing and rapid electrothermal heating. In contrast, screen-printed graphene inks on cotton deliver washable, low-voltage heaters that also function as sensitive strain sensors [86,87]. At the system level, recent e-textile reviews emphasise scalable processing and the healthcare relevance of graphene platforms for biomedical monitoring [13]. To improve skin–sensor coupling under dry and wet conditions, octopus-sucker-inspired micro-suction patterns were introduced onto graphene-coated fabrics (Fig. 10a). The SEM images show the surface morphology of PDMS-coated rGO fabric (Fig. 10b) and PDMS-coated rGO fabric with octopus-sucker-like micropatterns (Fig. 10c), which markedly enhance adhesion, enabling motion, ECG, and voice detection [88].

MXene-based strategies utilise hydrophilic $Ti_3C_2T_x$ for effective textile integration. Hybrid TOCNF/Ti_3C_2 inks permit 3D-printed fibres and fabrics that respond to mechanical and optical stimuli with high strain-sensing capabilities [89]. In parallel, highly conductive, machine-washable graphene e-textiles produced by industrial pad–dry–cure and compression maintain conductivity (~11.9 Ω sq.$^{-1}$) after repeated laundering [4], illustrating practical routes to scalable, affordable healthcare wearables [16]. Similarly, flexible $Ti_3C_2T_x$ MXene-based textile heaters fabricated by electrostatic self-assembly on APTES-treated PET fibres (Fig. 11a, c) showed reduced resistance and increased surface temperature with longer coating times. When stitched onto cotton gloves, they achieved ~53.5 °C under applied fields of 2.0–3.3 V cm^{-1} (Fig. 11e, f). Knitted MXene fabrics also maintained stable heating under deformation and, when worn on the wrist, safely elevated body temperature for wearable thermotherapy (Fig. 11g, h) [4].

For pressure sensing, electrostatically assembled MXene coatings on cotton create air-permeable, quick-response fabrics with a broad dynamic range, making them suitable for human–machine interfaces [90]. Core–shell MXene-based textiles with polydopamine adhesion layers and PDMS encapsulation combine super-hydrophobic breathability with photo-electro-thermal response and durable strain/temperature sensing for rehabilitation and sports feedback [91].

Hybrid architectures further expand functionality. Vapour-phase-polymerised PEDOT/MXene fabrics on cotton achieve low sheet resistance (≈3.6 Ω sq.$^{-1}$), high areal capacitance, strong Joule heating, EMI shielding (~36.6 dB), and strain sensing [92]. Complementarily, screen-printed graphene heaters on cotton operate at a few volts, remain machine washable, and provide strain-sensing capability [86]. Across MXene-textile designs, gauge factors span from ~4 in low-strain, durable MXene-containing cotton sensors, to very high values in engineered fibre/yarn systems (e.g., coaxial wet-spun MXene/PU fibres reporting GF ≈ 12,900 with ≤152% strain), while maintaining stability over 10^3–10^4 cycles; these figures enable detection of both subtle pulses and large-amplitude joint movements [93–95].

In sports analytics, wearable sensing platforms have recently leveraged the versatility of laser-induced graphene (LIG) for precise biomechanical monitoring. Raza et al. [96] reported the design of flexible and skin-conformal, LIG-based strain/pressure sensors integrated into elastic cotton sports fabrics through a simple transfer process from polyimide (PI) films onto stretchable polydimethylsiloxane (PDMS) (Fig. 12). When applied in volleyball, such textile-interfaced sensors demonstrated multifunctionality, enabling the detection of critical performance parameters, including arm position, ball contact during receptions, hitting force during spikes, and blocking events, all with real-time, on-body feedback. This multifunctional capability underscores the potential of LIG-enabled textile electronics to enhance both performance assessment and training strategies while simultaneously contributing to injury prevention by monitoring excessive joint load and impact forces [96].

According to Luo et al. [91] A $Ti_3C_2T_x$ MXene-based smart fabric was fabricated via a simple dip-coating process. The PM/PDMS textile, created as a core−shell structure, was photothermally active and exhibited exceptional electrothermal conversion, along with a top-notch

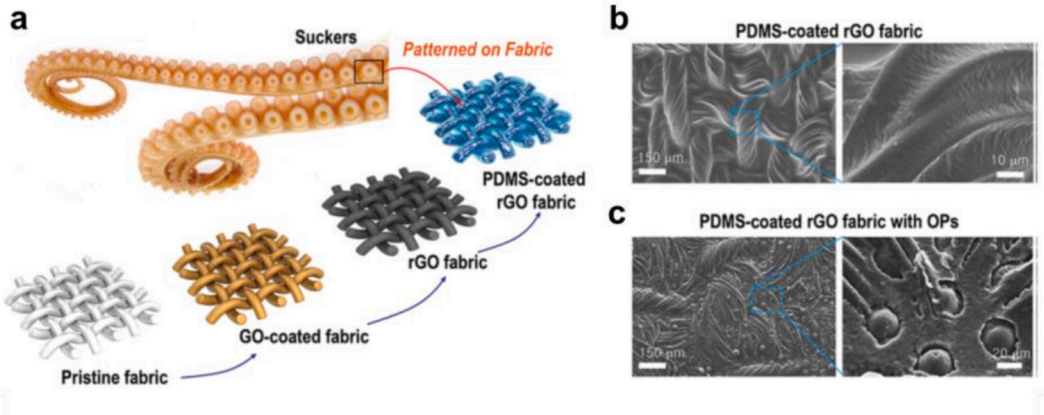

Fig. 10. Schematic of octopus-like, micro-suction patterns on rGO/PDMS-coated fabric: (a) Schematic illustration of the octopus-like patterned (OPs), rGO-fabric coated with rGO and PDMS. (b) Scanning electron microscope (SEM) images of plain fabric. (c) OP-engraved fabric. Reprinted with permission [88].

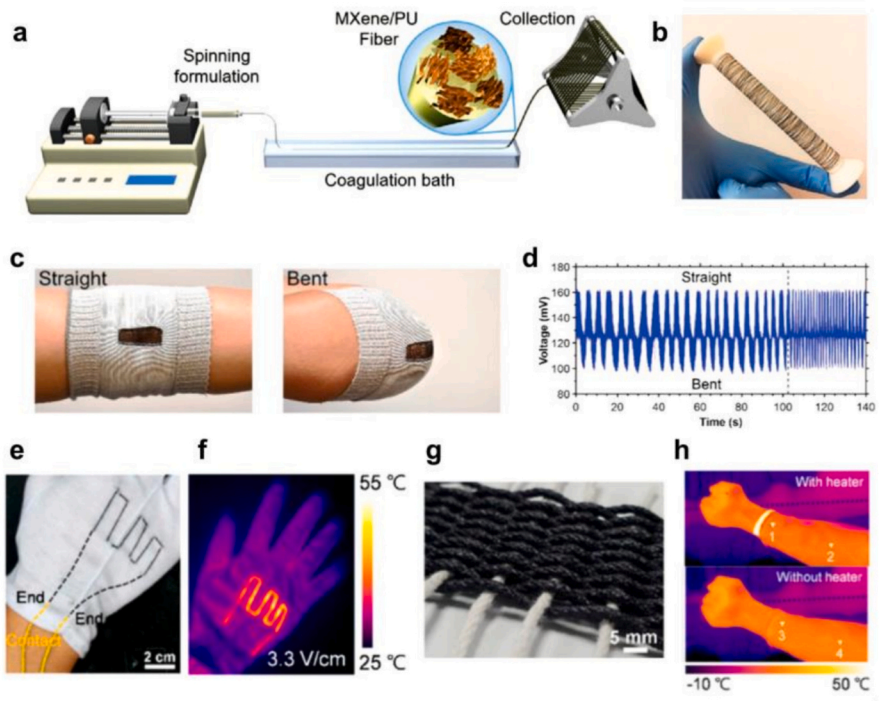

Fig. 11. (a) Schematic illustration of the wet-spinning process for MXene/PU fibres, involving extrusion of the spinning formulation into an isopropanol (IPA) coagulation bath, followed by fibre collection. (b) Photograph of a continuous ~100 m long MXene/PU fibre obtained via wet spinning. (c) Knitted elbow sleeve integrated with MXene/PU fibres, demonstrating flexibility under straight and bent states. (d) Real-time strain-sensing response of the sleeve during repeated elbow bending and straightening, highlighting stable voltage signals. (e) Cotton glove stitched with MXene-based fibre heaters. (f) Infrared thermal image of the glove showing uniform heat generation under an applied field of 3.3 V cm^{-1}. (g) Woven MXene textile heater, illustrating scalability and integration potential. (h) Infrared thermal images of the MXene fabric heater worn on an arm under sub-zero conditions, clearly demonstrating localized heating capability compared to the control without a heater. Adapted with permission [4].

thermal coefficient of resistance, as well as strain sensitivity. The construction and structural design process is illustrated in Fig. 13a, while the device's on-body applications for motion and temperature monitoring are depicted in Figs. 13b–g. The PM/PDMS textile has great potential for health monitoring, rehabilitation, and sports training applications due to its flexibility, breathability, and superhydrophobicity. However, more improvements are required to expand its sensing range and fully integrate it with electronic wearable systems.

Recently, MXene-based yarns have emerged as promising candidates for wearable strain-sensing applications due to their flexibility and electrical conductivity. In one representative example, dip coating is employed to fabricate a PU/MXene strain-sensing yarn, which is subsequently enhanced via magnetron sputtering and PDMS encapsulation [97]. The strain sensor exhibited a wide strain range of 200%, demonstrating excellent durability over more than 15,000 cycles and outstanding sensitivity, with a gauge factor exceeding 700. These features enabled reliable detection of both small- and large-scale human motion, demonstrating the potential of MXene-based yarns for next-generation health monitoring and smart textile applications.

Table 1 uses cross-material comparison to summarise the most representative 2D material textile strain/pressure sensors that have been discussed in this paragraph.

Across reported textile implementations, sensitivity improvements (high gauge factor) are repeatedly achieved through network-level

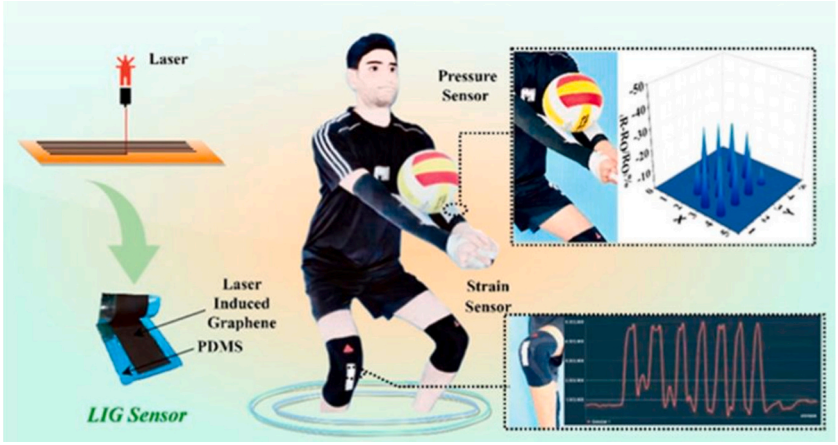

Fig. 12. LIG-textile sensing during volleyball actions (touch/spike) and signal traces. Reprinted with permission [96].

amplification strategies (microcrack engineering, porous/aerogel structures, hierarchical coatings), which can introduce trade-offs in hysteresis and mechanical robustness. Conversely, designs prioritising durability and washability tend to rely on stronger interfacial anchoring (binder/crosslinking chemistry) and encapsulation, which can reduce breathability and attenuate strain transfer. These observations suggest that for low-amplitude physiological signals, stable skin contact and low noise can be more decisive than peak sensitivity, whereas for large joint motion, mechanical integrity and repeatability under repeated deformation and laundering dominate [1,3].

3.3. ECG sensors

Textile-based dry electrodes are a practical alternative to gelled Ag/AgCl for continuous electrocardiography (ECG), enabling long-term, unobtrusive monitoring with improved comfort and reduced skin irritation. Screen-printed graphene on cotton or pre-treated fabrics achieves sheet resistances of ~42–100 Ω sq.$^{-1}$ and records ECG with high fidelity compared to Ag/AgCl (Pearson correlation ≈ 99.47%), while maintaining performance after repeated bending and laundering [27,98].

(see Table 2). Conducting polymer routes complement carbon electrodes. Screen-printed PEDOT:PSS on commercial finished textiles (with DMSO additive) provides dry-skin ECG with reduced skin–electrode impedance across 4–150 Hz, an improved signal-to-noise ratio under moisture/sweat conditions, and wash reusability [99]. Hybrid strategies in which graphene oxide (GO) underlayers are combined with PEDOT:PSS overcoats on knitted fabrics further lower interfacial impedance and enhance skin conformity for long-term ECG [100]. In garment-level implementations, pad–dry–cure graphene electrodes integrated into a washable sports bra demonstrate breathability and stability during human-motion monitoring [101].

Beyond single-function electrodes, fully printed graphene e-textiles integrate ECG/EEG recording with in-plane energy storage (≈ 3.2 mF cm^{-2}, ≥ 10.000 cycles) and remain machine-washable through suitable encapsulation schemes compatible with apparel processing [102]. For discreet placements, soft graphene textile electrodes positioned behind the ear enable ear-ECG suitable for robust HR/HRV extraction in hearable applications, illustrating unobtrusive form factors for continuous outpatient or daily life monitoring [103].

Overall, ECG textile electrodes based on 2D materials combine electrical conductivity, flexibility, and washability with high-quality biopotential recordings. However, future work should focus on improving mechanical–electrical stability over extended wear and developing skin–electrode interfaces that maintain low impedance under varying humidity and movement conditions. Additionally, real-time wireless data transmission and energy-autonomous operation remain important targets for next-generation smart textile ECG systems.

Table 2 summarises textile ECG electrodes based on 2D materials that have been discussed in this paragraph.

For biopotential electrodes, material selection is governed primarily by skin–electrode impedance stability, motion artefacts, comfort under prolonged wear, and wash durability rather than by conductivity alone. Graphene-based electrodes often provide robust conductive pathways and favourable chemical stability, whereas MXene-based electrodes can offer high conductivity and easy aqueous processing but may require more strict passivation to limit oxidation and performance drift under humidity/sweat exposure. Across both classes, the most reliable textile electrodes are typically achieved when 2D coatings are paired with textile-compatible binders/encapsulation strategies that preserve conformability and breathability while stabilising the interfacial contact over repeated wear and laundering [1,3,4].

3.4. Humidity and respiration sensors

Humidity and respiration sensors based on 2D materials offer high sensitivity, short response/recovery times, and seamless integration into textiles for on-body monitoring. MXene/AgNW coatings assembled layer-by-layer on silk fabric combine very low sheet resistance (~0.8 Ω sq.$^{-1}$), EMI shielding of approximately 54 dB (X-band), super hydrophobicity, and a pronounced humidity response, yielding breathable, multifunctional garments [104].

Graphene oxide (GO) coatings on nonwoven fabrics, prepared via a BSA-assisted process, deliver breathable, skin-friendly sensors that distinguish between fast and deep breathing, as well as spoken words without noticeable drift during prolonged use [105]. Likewise, GO on Coolmax® polyester, deposited by pad-dyeing, provides ultrafast humidity response and recovery while remaining largely insensitive to pressure and temperature fluctuations, which is promising for both activity and health monitoring [106].

For multifunctional operation, graphene woven fabrics (GWF) obtained via CVD and used as flexible conductive networks enable simultaneous sensing of humidity and temperature, supporting reliable physiological readouts in wearable formats [107].

At the fibre scale, Pt-decorated nitrogen-doped rGO (Pt-nRGO) fibres exhibit an extended humidity range (RH 6.1–66.4%) and ~ 1.36× sensitivity enhancement relative to undoped nRGO, offering an efficient route to compact, respiration-relevant humidity sensors suitable for textile integration and portable modules [108].

Collectively, these studies demonstrate that 2D-material-based humidity/respiration sensors can be adapted to diverse textile architectures (woven, knitted, nonwoven) and scalable finishing processes while preserving breathability, flexibility, and user comfort. Table 3 summarises representative examples of such systems, their substrates, fabrication methods, and key performance metrics.

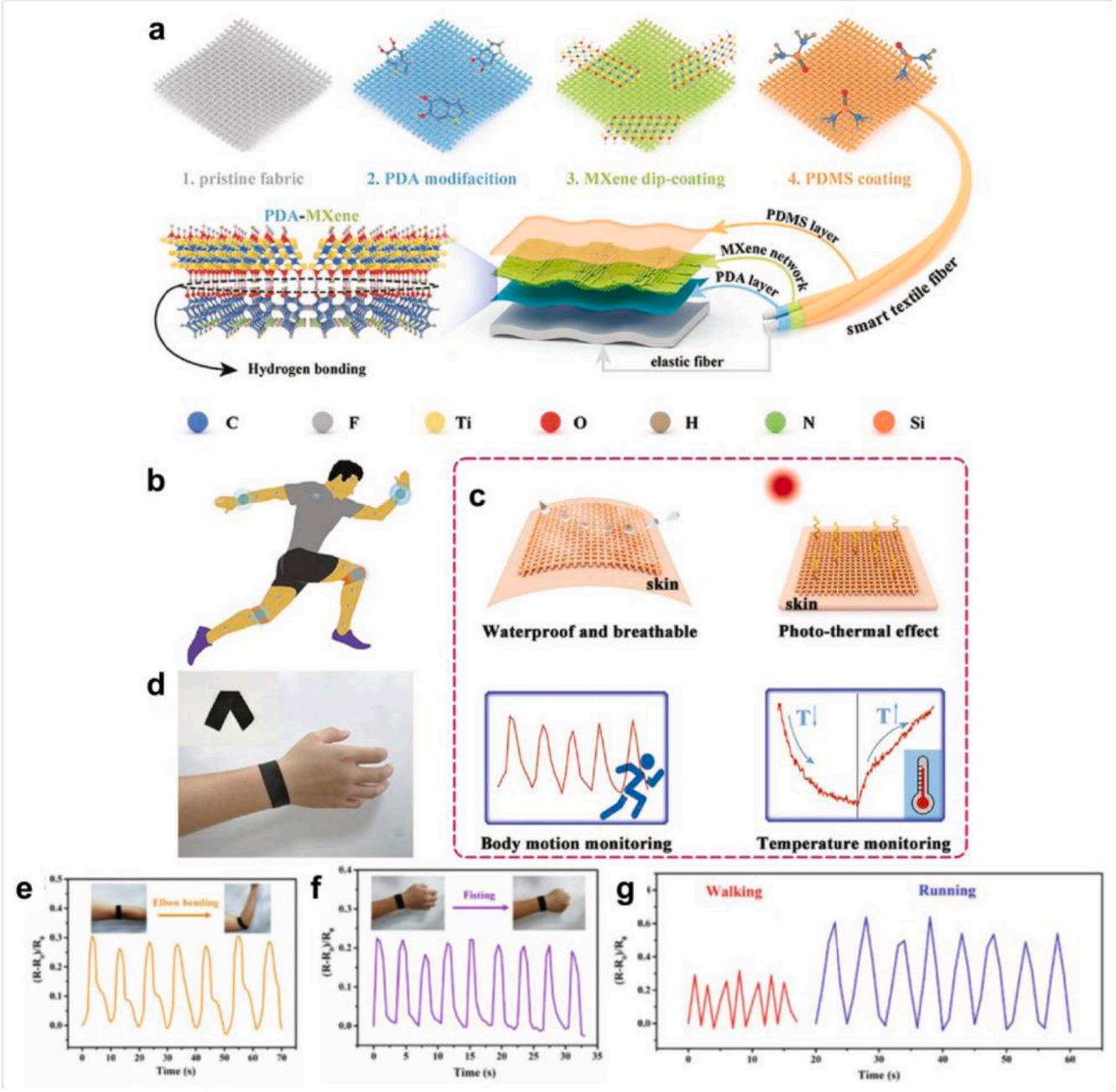

Fig. 13. Schematic diagram of fabrication methodology and structure of PM/PDMS textile. (b) Sketch of PM/PDMS textile on body joints for motion detection. (c) The PM/PDMS textile exhibits excellent performance as a smart strain sensor for several potential applications. (d) Photograph of a textile sensor worn on the wrist of a volunteer and an illustration of a bending textile. The textile sensor captures signals for monitoring (e) elbow bending, (f) fist clenching, and (g) walking and running. Adapted with permission [91].

3.5. Speech vibration/voice recognition sensors

Wearable sensors based on 2D materials can transduce subtle throat and facial muscle vibrations associated with speech. A seminal example is graphene woven fabrics (GWFs) transferred onto an elastic PDMS film to form a crack-mediated piezoresistive network. Under throat motion, controlled microcrack formation and propagation modulate resistance, enabling the recognition of letters, tones, words, and sentences with high separability of waveform signatures [109]. In this study, Wang et al. [109] clearly demonstrated throat-mounted GWF-on-PDMS sensors and outlined AI/DSP pipelines for speech recognition from muscle movement signals, whether or not a sound is produced.

Regarding textile substrates, an rGO-modified cotton pressure sensor fabricated by dipping/annealing provides a fully wearable platform that can be taped to the throat to capture speech-related muscle movements while also monitoring pulse and respiration; it reaches sensitivities up to 0.21 kPa^{-1} over a 0–500 kPa range with robust repeatability and attributes germane to garment integration and daily use [110].

Comparator devices and textile translations. Beyond conventional textile substrates, two wearable exemplars provide mechanistic comparators for bidirectional voice interfaces. An artificial throat based on laser-induced graphene (LIG) patterned on polyimide operates both as a piezoresistive detector of laryngeal vibrations and as a thermoacoustic emitter driven by Joule heating, enabling on-skin sound sensing and generation in a single platform [111]. A complementary skin-like artificial graphene throat (WAGT) formed by laser-scribed graphene on PVA

Table 1
Representative 2D material textile strain/pressure sensors (NR = not reported in the original paper).

Material/system (2D material retained)	Textile substrate (fabric/yarn)	Deposition/assembly	Binder/ encapsulation	Mode (strain/ pressure)	Key metrics (units)	Operating conditions	Durability	Ref.
MXene textile (PDA/PDMS core–shell)	Cotton fabric	Dip-coating: PDA modification to MXene deposition to PDMS topcoat (core–shell)	PDA; PDMS	Strain (also temperature)	Strain and temperature sensing indicated; quantitative strain metrics	NR	NR	[91]
Graphene ink/ cotton	Cotton fabric	Facial double-side screen printing (graphene ink on both sides)	Water-soluble polyurethane top layer (washability aid)	Strain (also Joule heating)	Conductivity ≈ 1.18 × 10^4 S m^{-1}; steady-state T ≈ 52.6 °C at 3 V; strain sensing reported	3 V (heating); strain-sensing test conditions	NR	[86]
MXene@cotton textile	Cotton fabric	Electrostatic adsorption of d-$Ti_3C_2T_x$ onto cotton fibres	NR	Strain	Gauge factor ≈ 4.11 (≤15% strain)	NR	>500 cycles	[93]
Ag/AgNW/ MXene conductive yarn	Elastic polyurethane-based yarn	Layered assembly: MXene coating to Ag nanoparticle sputtering to PDMS encapsulation (Ag/MXene/PU; PDMS/ Ag/MXene/PU)	PDMS encapsulation	Strain	Working strain up to ≈200%; GF >700; electrothermal capability noted	NR	>15,000 cycles	[97]
TOCNF/Ti_3C_2 MXene	Cellulose nanofibrils	3D printing/smart fibres and textiles using TOCNF–MXene ink	TOCNF (hybrid-ink rheology/ bridging component)	Strain (smart fibres/textiles; multi-stimulus)	High-sensitivity strain sensing	NR	NR	[89]
MXene/PU coaxial fibres	Polyurethane fibres (knittable into textiles)	Wet-spinning and coaxial wet-spinning (MXene/PU sheath with PU core)	PU matrix (sheath/core architecture)	Strain	Percolation ≈ 1 wt%; GF ≈ 12,900 (≈238 at 50% strain); sensing strain ≈ 152%	NR	Knitted textile stability reported in source	[94]
LIG (laser-induced graphene) fabric sensor	Textile-integrated LIG/ PDMS (sportswear integration)	Laser-induced graphene patterning; PDMS lamination/ encapsulation for strain/ pressure modules	PDMS (lamination/ encapsulation)	Strain/Pressure	Multifunctional sports monitoring	NR	NR	[96]
Graphene e-textiles	Polyester/cotton	Pad–dry–cure method with roller compression	Encapsulation of graphene flakes	Strain	Sheet resistance ≈11.9 Ω sq^{-1}; conductive after multiple home washes;	NR	NR	[16]
PEDOT/MXene on cotton	Cotton fabric	Vapour phase polymerisation and spray-coating	NR	Strain	Sheet resistance ≈3.6 Ω $sq.^{-1}$; areal capacitance ~1000 mF cm^{-2}; Joule heating ~193 °C at12 V; EMI SE ~36.6 dB	NR	NR	[91]
PANI/MXene fabric	Polyester fabric	Spray coating MXene	NR	Strain	All-solid-state supercapacitor 647 mF cm^{-2} (8.08 μWh cm^{-2}); GF 435; strain range 0–40.8%	NR	NR	[95]

Table 2
Textile ECG electrodes based on 2D materials.

Material/System	Textile substrate (type)	Process	Key outcomes	Ref.
Screen-printed graphene textile electrode	Cotton fabric (woven)	Screen printing of graphene ink	R_s ~ 42 Ω sq^{-1}; ECG comparable to Ag/AgCl (Pearson ≈99.47%); robust after bending/washing	[27]
Washable screen-printed graphene textile electrode	Pre-treated fabric (apparel grade) †	Thermal transfer + screen printing	Washable, flexible electrode; stable ECG after laundering; resistance tunable by print passes	[98]
Fully printed graphene e-textile (multifunctional)	Polyester–cotton blended fabric	Scalable printing + encapsulation	Machine-washable; ECG/EEG; in-plane supercapacitor ≈3.2 mF cm^{-2} (≥10,000 cycles)	[102]
Screen-printed PEDOT:PSS textile electrodes	Commercial finished textile (woven) †	Screen printing (PEDOT:PSS + DMSO)	Dry-skin ECG; reduced skin–electrode impedance (4–150 Hz); washable; SNR improves with moisture	[99]
GO + PEDOT:PSS coated knitted fabric	Knitted fabric †	Exhaust dyeing (GO) + LbL PEDOT:PSS coating	Flexible ECG electrodes; low impedance; improved skin conformity for long-term monitoring	[100]
Graphene-coated garment electrodes (sports bra)	Polyester knit (garment)	Pad–dry–cure (rGO), optional PEDOT:PSS over-coat	Highly flexible, breathable, washable; stable ECG during motion	[101]
Behind-the-ear graphene textile electrodes	Soft textile for hearables †	Soft graphene textile electrode integration	Discreet ear-ECG; robust HR/HRV extraction for hearables	[103]

Abbreviations: R_s, sheet resistance (Ω sq^{-1}); HR/HRV, heart rate/heart-rate variability; ECG/EEG, electrocardiography/electroencephalography.
† Substrate type not explicitly named in the source. Performance values are extracted from the cited sources; because test conditions vary across studies, comparisons are qualitative.

likewise delivers co-located detection and thermoacoustic emission with ultralight, conformal mechanics [112]. These mechanisms map onto textile embodiments via (i) lamination of ultrathin PI/PVA–LIG foils onto breathable fabric backings; (ii) in situ laser scribing on PI-coated

Table 3
Humidity and respiration of textile-based sensors.

Material/ System	Substrate/ Process	Key outcomes	Ref.
MXene/AgNW on silk	Silk fabric (woven). Layer-by-layer (LbL) assembly	R_s ≈ 0.8 Ω sq^{-1}; EMI SE ≈ 54 dB (X-band); superhydrophobic; sensitive humidity response; breathable	[104]
GO/nonwoven (BSA-assisted)	Nonwoven fabric (NWF)† BSA-assisted GO coating	Breathable, skin-friendly; distinguishes fast/deep breathing and spoken words; stable over prolonged use	[105]
GO/Coolmax®	Coolmax® polyester (knit/ woven). Pad-dyeing	Ultrafast response/recovery; insensitive to pressure/ temperature; activity & health monitoring	[106]
Graphene woven fabric (GWF)	Graphene woven network (free-standing) † CVD-grown GWF used as a flexible network	Simultaneous humidity & temperature sensing; flexible device; low cross-sensitivity	[107]
Pt-nRGO fibre	Graphene fibre on colorless polyimide film † N-doping + Pt anchoring	RH range 6.1–66.4%; ~1.36× sensitivity gain vs nRGO; breath monitoring	[108]

† Substrate not specified verbatim as a conventional textile in the source.

fabrics to form LIG patterns directly on cloth; (iii) transfer printing of patterned films onto knitted bases using TPU/PDMS adhesive webs; and (iv) modular appliqué patches positioned at the collar/scarf region to maintain robust throat contact while preserving washability. In all cases, micro-perforated encapsulants and serpentine interconnects help maintain drape, air permeability, and electrical insulation under repeated use. In summary, 2D-material voice sensors span crack-based GWF films, rGO-textile composites, and LIG/WAGT artificial throats, covering silent-speech capture, robust waveform discrimination, and even sound generation, with clear routes towards textile integration (Table 4).

3.6. Body temperature sensors

Textile-based temperature sensors have progressed from bulky, wire-based probes to lightweight, flexible, and strain-tolerant architectures by leveraging 2D carbons directly on yarns and fabrics. Graphene-coated polypropylene (PP) textile fibres display a negative temperature coefficient of resistance (TCR) over the 30 °C–45 °C range and can operate at ~1 V while maintaining mechanical stability and washability, features that support direct garment integration [113]. At the fabric scale, graphene/alginate composite nonwoven sensors exhibit high sensitivity and strong immunity to strain and humidity interference, with a temperature accuracy of around 0.1 °C during skin-mounted tests, highlighting their dependability for everyday use [114].

On the fibre level, a skin–core composite, temperature-sensing fibre, PEDOT:PSS core encapsulated by polyurethane/graphene, achieves −1.72% $°C^{-1}$ sensitivity, 0.1 °C resolution, ~17 s response, and anti-sweat interference; importantly, the fibres are braidable with commercial cotton yarns to realise fabric-level, continuous body-temperature monitoring [115]. Although not a sensor per se, graphene glass-fibre fabric (GGF) heaters offer high emissivity (~0.92) and thermal radiation efficiency (~79.4%) with ultrafast heating, providing thermotherapy and thermal management modules that complement textile temperature sensing in healthcare wearables [116]. Representative systems and metrics are summarised in Table 5.

Table 4
Speech/voice sensors based on 2D material.

Material/System	Substrate/Process	Key outcomes	Ref.
Graphene woven fabric (GWF) throat sensor	Elastic PDMS film † CVD-grown GWF transferred to PDMS; crack-mediated piezoresistive sensing	Throat-mounted; recognizes letters/tones/ words/sentences; enables silent-speech capture; AI/DSP-ready signals	[109]
rGO–cotton throat/ pressure sensor	Cotton fabric (absorbent cotton) Dip coating in GO followed by thermal reduction (annealing)	Captures speech-related throat motion; also, pulse/respiration; sensitivity up to 0.21 kPa^{-1} (0–2 kPa); range to 500 kPa	[110]
LIG artificial throat (detect & emit)	Polyimide (PI) film † One-step laser-induced graphene on PI; thermoacoustic emission	Detects laryngeal vibrations; generates sound (100 Hz–40 kHz); wearable patch for assistive voice	[111]
Wearable skinlike artificial graphene throat (WAGT)	Poly(vinyl alcohol) (PVA) film † Laser-scribed graphene on PVA; water-assisted transfer; dual-mode detection + emission	Ultra-sensitive detection; co-located thermoacoustic emission; conformal & ultralight for perithyroid placement	[112]

3.7. Cross-material selection criteria and translation constraints (scalability and reproducibility)

A consistent pattern across healthcare e-textiles is that laboratory demonstrations often optimize one aspect (e.g., peak sensitivity) while under-reporting critical translation parameters (wash protocols, inter-batch reproducibility, and stability under sweat/humidity). For textile finishing, selection of 2D materials can be guided by four coupled criteria: (i) target function and required interface (skin electrode vs environmental interface), (ii) processability into stable inks/coatings compatible with textile manufacturing, (iii) durability envelope (bending/fatigue and laundering) and failure modes (delamination, oxidation, network fragmentation), and (iv) user-facing constraints (breathability, comfort, and long-term skin-contact stability) [1,3].

From this perspective, graphene-derived finishes are often preferred when oxidation tolerance and mechanically stable conductive networks are important, whereas MXenes are attractive for low-voltage, high-conductivity coatings, provided that environmental stability is achieved through termination control, passivation, and encapsulation. Semiconducting TMDs and BP are most compelling when semiconducting/ piezoelectric behaviour is required, but they typically demand additional interface engineering (hybridisation, protective layers) to meet garment-level durability targets [3,4,37].

Finally, scalability and reproducibility are treated explicitly as translation constraints: textile-relevant routes preferentially rely on liquid-phase processing and finishing methods with established industrial compatibility, and reported performance is most convincing when supported by (a) defined washing standards (programme and number of cycles), (b) cyclic fatigue tests under relevant strains, and (c) stability tests under humidity/sweat exposure with performance retention metrics [1,3].

4. Active functionalisation of textiles with 2D materials for healthcare applications

Unlike the passive devices discussed in Section 3, which monitor physiological signals without influencing the wearer's state, this section focuses on active textile systems in which 2D materials enable controlled thermal regulation, targeted stimulation, and other on-demand therapeutic functions. Due to their ultrathin form factor, high electrical and thermal conductivity, and tunable optoelectronic properties, 2D materials can be integrated into garments while maintaining drape and breathability. This enables thermotherapy modules (Joule/photothermal), electro-/thermo-stimulation interfaces, and triggerable

Table 5
Body temperature textile sensors based on 2D materials, normalized metrics, and test conditions. The GGF entry is retained as a thermal-management comparator for healthcare garments (NR = not reported in the original paper).

2D material/system	Substrate (fabric/yarn)	Deposition/Assembly	Binder	Function	Key metrics (units)	Operating conditions	Durability	Ref.
Graphene-coated PP textile fibres (CVD TLG/SEG)	Polypropylene (PP) fibres	Coating/lamination; carbon-paste contacts	NR	Thermistor-like (NTC)	Negative TCR (30–45 °C); operates ~1 V	Ambient (not specified); ~1 V	Washability reported	[113]
Graphene/alginate composite nonwoven	Nonwoven fabric	Composite formation + coating	NR	Resistive temperature sensing	Accuracy ~0.1°C; anti-interference to strain/humidity	Ambient (not specified)	NR	[114]
PU/graphene-encapsulated PEDOT:PSS fibre (skin–core)	Composite fibre; braid-integrated with cotton yarns	Wet-spun PEDOT:PSS core; PU/graphene encapsulation	PU	Resistive temperature sensing	Sensitivity −1.72% °C^{-1}; resolution 0.1 °C; response ~17 s; anti-sweat	Ambient (not specified)	NR	[115]
Graphene glass-fibre fabric (GGF)	Glass-fibre fabric (woven)	CVD-grown graphene; dual-emitter radiant heater	NR	Radiant heating (comparator)	Emissivity ≈ 0.92; radiation efficiency ≈ 79.4%; ultrafast heating	Electrical bias (not specified)	NR	[116]

Notes:
1. Metrics are reported as stated in the cited articles; TCR is the temperature coefficient of resistance.
2. Electrical units are normalized as sheet resistance (Ω/□), voltage (V), and time (s); temperature is reported in °C.
3. Laundry durability, when available, should specify the test programme (e.g., ISO 6330 or AATCC 135: temperature, time, number of cycles).
4. If only 'washable' is reported in the source, it is indicated qualitatively.

therapeutic finishes [1,3].

Proof-of-concept studies have already demonstrated low-voltage, rapid, and spatially uniform heating on fabrics, e.g., $Ti_3C_2T_x$-MXene textiles for healthcare thermotherapy and dual-emitter graphene–glass-fibre fabrics for radiant thermal management, highlighting realistic pathways to wearable intervention platforms [116,117].

Compared to passive sensors, active garments must satisfy additional system-level requirements: (i) power management and thermal dose regulation; (ii) safety during prolonged skin contact (temperature limits, leakage current, EMI); (iii) resistance to sweat and humidity; and (iv) mechanical stability under bending, stretching, and repeated washing. The remainder of this section organises the field around three application pillars: textile heaters for thermotherapy, active (electro/thermo/opto) stimulation, and on-fabric therapeutic release, with an emphasis on material/processing choices, device architectures, durability, and clinical relevance [1,3].

4.1. *Wearable thermotherapy*

Textile heaters based on 2D materials are increasingly favoured for wearable thermotherapy, localized temperature regulation, and rehabilitation support because they combine low areal weight, high flexibility, mechanical durability, and uniform heat distribution with fabric breathability. Screen-printed graphene inks on woven cotton produce

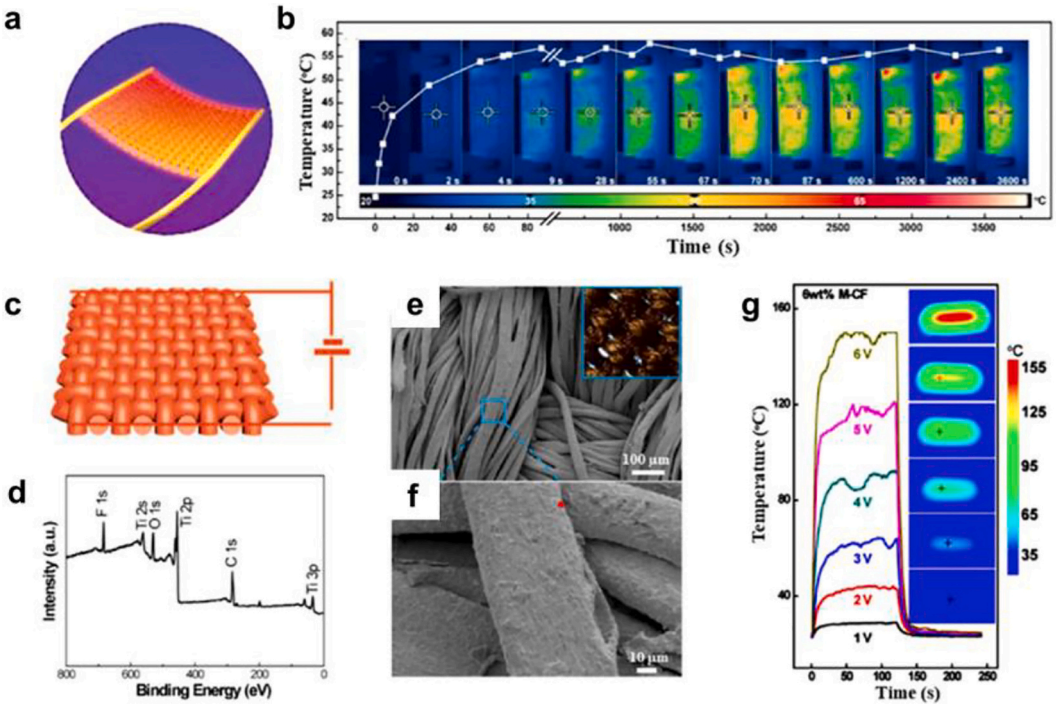

Fig. 14. Representative heater architectures and textile integration pathways with 2D materials. (a) Schematic Joule-heating textile; (b) a time-dependent temperature profile at a constant potential of 3 V for a silicone-coated MXene textile; (c) Schematic illustration of MXene-coated cotton fabric used in Joule heating; (d) XPS spectra of $Ti_3C_2T_x$; (e, f) optical microscope and SEM images of 6 wt% MXene-coated cotton fabric; and (g) time − temperature profile of 6 wt% MXene coated cotton fabric under 1 to 6 V. Reprinted with permission [4].

wash-durable heaters that reach ~52.6 °C, at ~3 V, while retaining strain-sensing capability, attributes essential for thermally active garments that also monitor motion [86]. Laminated PEDOT/MXene textiles fabricated by vapour-phase polymerisation (PEDOT) and spray-coating of $Ti_3C_2T_x$ deliver low sheet resistance (≈3.6 Ω sq.$^{-1}$), efficient Joule heating (≈ 193.1 °C at 12 V), and concurrent EMI shielding and strain sensing, illustrating multifunctionality on cotton fabrics [92].

Direct functionalisation of fabrics with $Ti_3C_2T_x$ MXene by dip-coating yields breathable, flexible heater textiles with rapid, spatially uniform Joule heating intended for garment-level healthcare and medical therapy scenarios [117]. In parallel, graphene glass-fibre fabrics grown by CVD act as high-emissivity radiant heaters (ε ≈ 0.92; thermal radiation efficiency ≈ 79.4%), with an ultrafast electrothermal response and uniform temperature fields, which are useful where radiant, rather than purely convective, heating is preferred. A further representative system based on PPy-modified MXene on polyester, sealed with a thin silicone overcoat, combines water resistance, outstanding EMI shielding, and moderate-voltage Joule heating, making it suitable for personal thermal management [118]. As shown in Figs. 14a–b) [4], this design had flexibility and stable heating to ~79 °C, at 4 V [118]. Likewise, MXene-coated cotton fabrics (Figs. 14c–g) had strong bonding and tunable heating from 29 °C to 150 °C, at 1–6 V, thus having a huge application in wearable heaters [119]. In healthcare, heating performance must be balanced with safety. Prolonged skin contact at temperatures around the low to mid-40 °C range is commonly targeted. Experimental and clinical evidence indicate that pain perception begins at temperatures just above 43 °C, and superficial burn injury occurs when the basal epidermis reaches ~44 °C, underscoring the need for careful control and feedback in wearable heaters [120,121].

Table 6 summarises representative heater textiles used in wearable healthcare contexts.

4.2. Self-powered and energy-harvesting textile devices based on 2D materials for healthcare applications

Functionalising textiles with 2D materials enables self-powered platforms that harvest biomechanical or thermal energy while remaining lightweight, breathable, and conformal. On the triboelectric side, graphitic carbon nitride (g-C_3N_4) nanosheets decorated with Ag nanoparticles on carbon-cloth electrodes, separated by a nylon interlayer, form a textile triboelectric nanogenerator (T-TENG) that delivers open-circuit voltages on the order of ~200 V, charges commercial capacitors, and harvests energy from finger, wrist, and hand motions, showing clear routes to garment integration [80].

MXene-textile architectures likewise provide effective electrodes for cloth-based TENGs. $Ti_3C_2T_x$ supported by cotton fabric serves as a flexible electrode layer for self-powered sensing, underscoring the value of 2D metallic carbides/nitrides in wearable harvesters [122]. Within graphene platforms, ultrasonic, spray-coated graphene electrodes on woven/knit fabrics yield fabric-based TENGs with scalable processing and robust motion-sensing/harvesting performance [123].

Beyond triboelectrics, thermoelectric harvesting from low-grade body heat has been realised on cloth via pad–dry–cure, layer-by-layer coatings of rGO (n-type) and PEDOT: PSS (p-type), producing wearable textile TEGs that generate tens to >100 mV under realistic ΔT and remain compatible with fabric mechanics, promising energy-autonomous, health-monitoring nodes [124]. Collectively, these exemplars demonstrate that 2D material finishes can serve as both functional electrodes and active conversion layers on textiles, thereby reducing reliance on bulky batteries in wearable healthcare (Table 7).

4.3. Photothermal and photonic functionalities in healthcare textiles based on 2D materials

The photothermal and photonic properties of 2D materials are being increasingly leveraged to engineer healthcare textiles that provide controlled thermal management, light-assisted therapy, and optical modulation. Materials such as MXenes, graphene and its derivatives, and transition-metal dichalcogenides (TMDs) exhibit strong light–matter interaction and efficient light-to-heat conversion, enabling on-garment warming, sterilization, and thermal stimulation, while preserving breathability and drape. In parallel, electro-optical control of emissivity using graphene enables photonic textiles that regulate radiative heat exchange or support optical signalling. When integrated onto cotton, silk, polyester, and blended fabrics using dip-coating, reduction, or lamination, these systems maintain performance under bending and laundering, which is essential for repeatable, skin-safe use in daily wear.

Representative examples include: (i) superhydrophobic, breathable textiles containing Mxene that demonstrate strong photothermal and electrothermal responses on fabric substrates, making them suitable for on-body warming and versatile wearable applications [91]; (ii) reduced graphene oxide (rGO) on silk fabrics that deliver high solar photothermal conversion with durability and washability, illustrating how textile architecture (capillarity, permeability) amplifies light-to-heat performance [125]; and (iii) MoS_2-modified polycotton fabrics that rapidly self-heat under sunlight to enable photothermal disinfection while retaining antibacterial efficiency after repeated washing, an immediately relevant healthcare function for reusable protective

Table 6
Representative textile heaters based on 2D materials for healthcare applications, normalized metrics, and test conditions (NR = not reported in the original paper).

2D material/ system	Substrate (fabric/yarn)	Deposition/Assembly	Function	Key metrics (units)	Operating conditions	Durability	Ref.
Graphene/ cotton fabric	Woven cotton	Double-side screen-printing of graphene inks	Joule heating (wash-durable)	~52.6°C @ ~3 V; also strain sensing	Electrical bias ~3 V	Machine-washable	[86]
$Ti_3C_2T_x$ MXene fabric	Cotton/ nonwoven fabrics	Dip-coating functionalisation	Joule heating (breathable fabric)	Fast, uniform low-voltage heating	Low-voltage operation (exact V not specified)	NR	[117]
PEDOT/MXene textile	Cotton fabric	Vapour-phase polymerisation (PEDOT) + spray-coated MXene laminated film	Joule heating + EMI shielding + strain sensing	R□ ≈ 3.6 Ω/□; T ≈ 193.1 °C @ 12 V; EMI SE ≈ 36.6 dB	Electrical bias 12 V	NR	[92]
Graphene glass-fibre (GGF) fabric	Glass-fibre fabric (woven)	CVD-grown graphene (dual-emitter radiant heater)	Radiant heating (high emissivity)	Emissivity ≈ 0.92; radiation efficiency ≈ 79.4%; ultrafast response	Electrical bias (not specified)	NR	[116]
PPy/MXene on polyester	Woven polyester	In-situ PPy on MXene + thin silicone coating	Joule heating + EMI shielding	Moderate-voltage heating; high EMI shielding	Electrical bias (not specified)	Water-resistant	[118]

Notes:
1. Metrics are reported as stated in the cited articles; temperature rise is reported as surface temperature (°C), unless otherwise specified.
2. Electrical units are normalized as sheet resistance (Ω/□), voltage (V), and time (s); temperature is reported in °C.
3. Laundry durability, when available, should specify the test programme (e.g., ISO 6330 or AATCC 135: temperature, time, number of cycles).
4. If only 'machine-washable' or 'water-resistant' is reported in the source, this is indicated qualitatively.

Table 7
Representative self-powered and energy-harvesting textile devices using 2D materials for healthcare applications, normalized metrics, and test conditions (NR = not reported in the original paper).

2D material/system	Substrate (fabric/yarn)	Deposition/Assembly	Function	Key metrics (units)	Operating conditions	Durability	Ref.
g-C_3N_4/AgNPs TTENG (with nylon interlayer)	Carbon cloth	Dip-coated g-C_3N_4 nanosheets + AgNPs; nylon interlayer	Triboelectric nanogenerator (textile T-TENG)	Open circuit ~200 V; charges commercial capacitors; harvests finger/wrist/hand motions	Human motion; ambient	NR	[80]
$Ti_3C_2T_x$ MXene fabric electrode for TENG	Cotton fabric	MXene-coated/support electrode	Triboelectric nanogenerator (textile electrode)	Flexible textile TENG; self-powered sensing; stable cloth-based electrode performance	Human motion; ambient	NR	[122]
Graphene-electrode fabric TENG	Woven/knit fabrics	Ultrasonic spray-coated graphene electrodes	Triboelectric nanogenerator (fabric-based)	Scalable fabric-based TENG; wearable energy harvesting and motion sensing	Human motion; ambient	NR	[123]
rGO/PEDOT:PSS thermoelectric textile (TEG)	Cotton fabric	Pad–dry–cure layer-by-layer coatings (rGO n-type, PEDOT:PSS p-type)	Thermoelectric generator (TEG)	Generates tens to >100 mV under realistic ΔT; fabric-compatible and flexible	Low-grade body heat; ΔT across cloth	NR	[124]

Notes:
1. Metrics are reported as stated in the cited articles. For triboelectrics (TENGs), open-circuit voltage (V_oc) and qualitative output descriptors are used when detailed values are not reported in the manuscript.
2. For thermoelectrics (TEGs), voltage is reported under realistic temperature gradients (ΔT) across textiles.
3. Electrical units are normalized as voltage (V) and time (s), where applicable. If laundry durability is stated qualitatively in the source, it is indicated as such.

garments [126]. Beyond pure heating, (iv) multilayer-graphene devices laminated onto fabrics achieve voltage-tunable infrared emissivity via reversible ion intercalation, establishing a photonic textile platform for dynamic thermal regulation and IR communication [127]. Finally, (v) electrospun membranes incorporating black phosphorus (BP) demonstrate light-responsive wound-care architectures compatible with skin-contact dressings and can be translated into textile-adjacent patches [128].

Beyond material selection, photothermal/electrothermal textile performance is governed by architecture-level choices that determine heat localisation, air permeability, and durability under bending and laundering. For 2D-material-based heaters, key design variables include: nanosheet network topology (sheet size/loading/percolation), the binder or crosslinking strategy that anchors coatings to fibres, the degree of encapsulation required to suppress oxidation and wash-off while preserving breathability, and the placement of conductive pathways (surface-coated yarns, coated fabrics, or patterned tracks). Fig. 15 summarises these variables that connect finishing choices to healthcare-relevant outcomes such as stable Joule heating under cyclic strain, skin-safe temperature control, and repeatability after washing [1,3,4].

An adaptive smart fabric incorporating $BaSO_4$ particles and rGO-wrapped thermochromic microcapsules (G-TM) was identified as a key example of photothermal–photonic synergy in 2D material-based textiles. This dual-modal fabric offers consistent thermal comfort across different climates by enabling radiative cooling at high temperatures and solar heating at low temperatures. Fig. 16 shows how spectrally

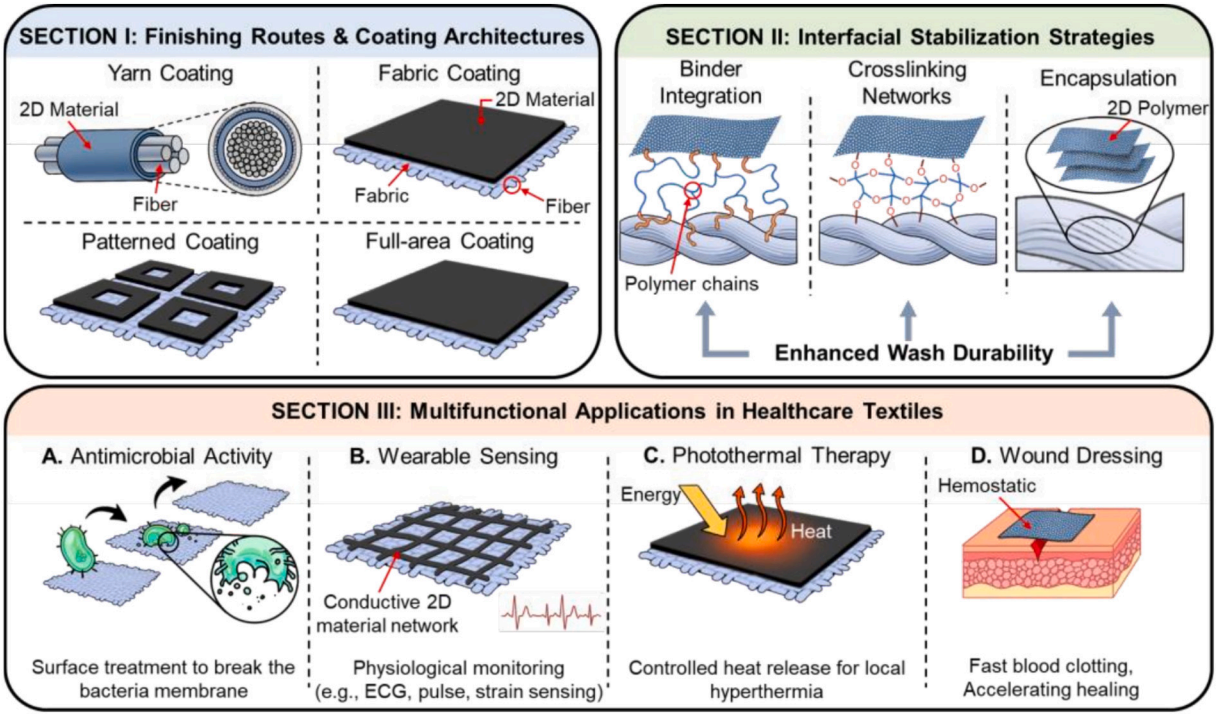

Fig. 15. Schematic overview of (I) finishing routes and coating architectures (yarn/fabric; patterned vs full-area), (II) interfacial stabilisation strategies (binder/crosslinking/encapsulation) governing wash durability and mechanical fatigue resistance, and (III) multifunctional applications (antibacterial activity, physiological monitoring, photothermal therapy, wound dressing) [1,3].

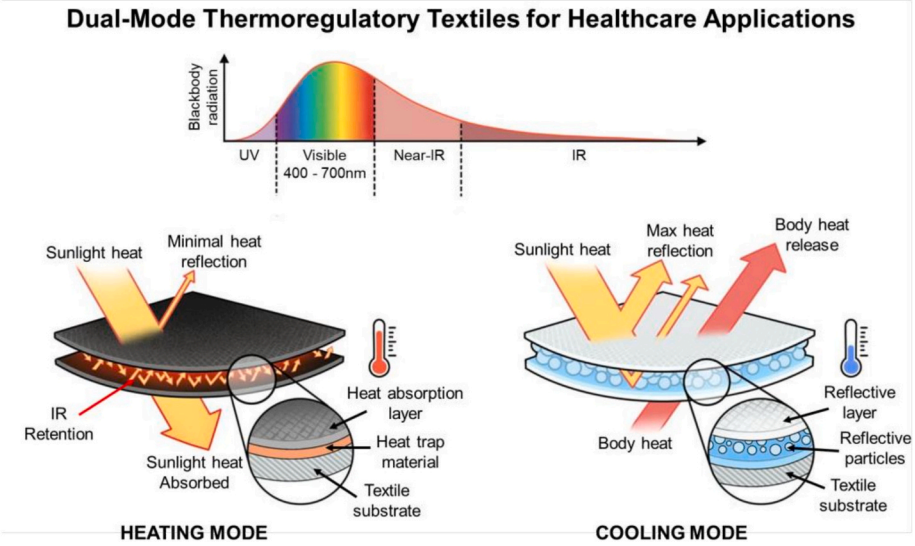

Fig. 16. Schematic representation of dual-mode thermoregulatory textiles relevant to healthcare wear. The schematic highlights the functional principle (heating vs cooling via spectral selectivity) and the corresponding textile-integration levers (layer placement, encapsulation for durability, and comfort constraints), as summerised from recent smart-textile literature [1,3].

selective components and 2D-material coatings can be integrated as textile-compatible layers without compromising wear comfort [3].

Such temperature-adaptive textiles showcase the potential of 2D-material-enhanced fabrics for healthcare applications that require precise thermal management and user comfort [129].

Collectively, these demonstrations indicate that the photothermal and photonic functions of 2D materials can be integrated through conventional textile processing to yield garments with self-heating, self-disinfecting, and emissivity-modulated properties for therapeutic applications and continuous monitoring (Table 8).

4.4. Triboelectric and piezoelectric textile sensors based on 2D materials for self-powered healthcare applications

Self-powered textile sensors integrate energy harvesting and active sensing into a single platform, enabling continuous physiological monitoring without the need for external power packs. In healthcare, such systems are attractive for long-term ambulatory tracking, rehabilitation feedback, cardiorespiratory surveillance, and fall-risk alerts. Two-dimensional materials, most notably MXenes, graphene, and MoS_2, provide high surface area, tunable surface chemistry, and mechanical compliance, thereby enhancing both triboelectric output and sensing responsivity when applied to cotton, silk, or synthetic fibres via dip-coating, printing, electrospinning, or in situ polymerisation.

Table 8
Representative photothermal and photonic healthcare textile devices based on 2D materials (NR = not reported in the original paper).

2D material/ system	Substrate (fabric/yarn)	Deposition/Assembly	Binder	Function	Key metrics (units)	Operating conditions	Durability	Ref.
$Ti_3C_2T_x$ MXene textile	Cotton/ breathable fabric	PDA adhesion layer + MXene decoration; multi core–shell architecture	PDA	Electro-/ photothermal warming	Breathable, superhydrophobic; stable electro-/ photothermal response	Ambient; electrical bias and/or sunlight	NR	[91]
rGO–silk photothermal fabric	Silk fabric (woven)	Graphene oxide coating + chemical reduction (rGO)	NR	Solar photothermal heating	High solar photothermal conversion (1 sun); flexible platform	Sunlight	Durable, washable (qualitative)	[125]
MoS_2-modified antibacterial fabric	Polycotton fabric	MoS_2 nanosheet finishing/coating	NR	Photothermal self-disinfection	Sunlight-driven rapid heating enabling photothermal self-disinfection	Sunlight	Antibacterial efficacy retained after washing (qualitative)	[126]
Graphene adaptive IR textile (emissivity-tunable)	Textile backing with laminated multilayer graphene	Lamination + electrolytic gating for voltage-tunable IR emissivity	NR	Photonic textile (IR emissivity modulation)	Dynamic thermal regulation and IR signalling on fabric	Voltage-controlled emissivity (ambient)	NR	[127]
BP-containing electrospun membrane (textile-adjacent)	Electrospun asymmetric wettable membrane	Electrospinning with black phosphorus (BP) and Rg1; surface design for wound contact	NR	Light-responsive wound-care patch	Enhanced infected-wound healing; compatible with textile-adjacent use	Light stimulation; wound-contact environment	NR	[128]

Notes:
1. Photothermal metrics refer to solar illumination at 1 sun when stated by the source; IR-photonic performance is described via emissivity modulation (dimensionless).
2. Electrical/thermal units are reported as stated in the cited articles; temperature is in °C. If laundry durability is stated qualitatively in the source, it is indicated as such.
3. Textile-adjacent wearable patches rather than conventional fabrics; included to illustrate mechanisms and translation pathways towards textile embodiments

Using $Ti_3C_2T_x$ MXene supported on cotton fabric as the electrode layer, textile-based triboelectric nanogenerator (TENGs) achieve robust outputs suitable for self-powered motion sensing, demonstrating clear detectability of large-amplitude limb movements, as well as subtle biomechanical cues (e.g., gait phases) in wearable form factors [122]. Within graphene platforms, ultrasonic spray-coated graphene electrodes on woven/knit fabrics provide scalable, conformable TENGs that harvest energy from joint bending and steps while serving as motion sensors for rehabilitation analytics [123].

Furthermore, incorporating 2D fillers into PVDF transducers can enhance low-frequency physiological sensing (e.g., breathing and plantar pressure). MoS_2-embedded PVDF hybrid films, made by bar-printing and self-poling, enhance triboelectric performance in flexible wearables and can be integrated into textiles via coating or lamination onto fabric backings [130]. In parallel, hexagonal boron-nitride (h-BN) nanosheets blended into PVDF nanofibre mats yield high-output piezoelectric nanogenerators (PENGs) that are compatible with low-cost fabrication. These mats are readily mounted onto garments or integrated into multilayer textile patches for pressure/strain sensing [131]. Collectively, 2D material finishes enable battery-lean health wearables in which the same textile architecture can both harvest energy and sense movement (Table 9).

In wearable healthcare textiles, triboelectric nanogenerators (TENGs) have shown great promise as self-powered sensing and energy harvesting devices. Because of their high conductivity, electronegativity, and flexibility, MXenes, especially those based on Ti_3C_2, can be integrated into a variety of TENG components (Fig. 17). MXenes' versatility and potential for developing multifunctional, photothermal, and photonic healthcare textiles are demonstrated by their use as conductive films, triboelectric layers, polymer fillers, and charge-trapping interfaces [132].

5. Outlook and future perspectives

The integration of two-dimensional (2D) materials into textile platforms for healthcare has progressed rapidly, yielding flexible, lightweight devices capable of real-time physiological monitoring and, increasingly, on-garment actuation. As summarised in this review, graphene derivatives, MXenes, transition-metal dichalcogenides (TMDs), h-BN, and related 2D systems can be processed in a compatible manner on cotton, polyester, silk, and blended fabrics via dip-coating, pad–dry–cure, printing, electrospinning, and hybrid assembly strategies. These approaches underpin wearables for strain/pressure sensing, ECG, respiration/humidity, temperature monitoring, and self-powered operation. Looking ahead, several scientific and translational priorities merit focused attention. Accordingly, six interdependent priorities can be delineated, such as scalable synthesis with atomic-level control; environmental stability and passivation; rational chemical modification; metrology, reliability, and washability standards; manufacturing and system integration; and safety, biocompatibility, and data stewardship, as detailed in points (i)–(vi) below.

(i) Scalable synthesis with atomic-level control. For clinical-grade e-textiles, it is essential to achieve wafer- or roll-scale 2D films and inks with uniform composition, phase, and defect density, as well as deterministic control of alloying and sharply defined lateral/vertical heterojunctions. Comprehensive roadmaps and perspectives emphasise that advancing chemical vapour deposition (CVD/ALD/MBE), solution growth, and deterministic transfer must go hand-in-hand with contamination-minimising, roll-to-roll-compatible integration to ensure reproducibility and yield [28,35,36].

(ii) Environmental stability and passivation. Air- and moisture-sensitive materials (e.g., black phosphorus) demand robust passivation. In situ and plasma-enhanced ALD studies of Al_2O_3 on BP clarify nucleation chemistry and demonstrate effective degradation suppression under ambient conditions; complementary work details oxidation pathways and long-term stabilisation strategies (e.g., ionic-liquid/encapsulation routes) [133]. For MXenes, surface terminations (–O/–OH/–F, occasionally —Cl) and oxidation kinetics critically govern hydrophilicity, electronic transport, and redox behaviour; authoritative overviews and textile-focused reviews outline routes to control terminations and preserve conductivity in fabrics [4,134].

(iii) Rational chemical modification. Heteroatom doping, intercalation, and targeted surface functionalisation remain powerful tools for tuning carrier density, Fermi-level position, excitonic interactions, and catalytic activity, while improving dispersion stability and fibre adhesion. A broad materials-palette perspective details these levers across 2D families and highlights their implications for device performance and durability, principles directly translatable to textile finishes and inks [31].

(iv) Metrology, reliability, and washability standards. Closing the lab-to-clinic gap requires traceable metrology for defects, dopants/intercalants, interfaces, and contact resistance correlated to drift, hysteresis, and noise in textile device operation. Field-spanning reviews stress the need for multimodal characterisation linked to performance metrics [35]. In parallel, realistic laundering, perspiration, abrasion, and flex-fatigue protocols should align with textile standards; the

Table 9
Triboelectric and piezoelectric textile sensors based on 2D materials, normalized metrics, and test conditions (NR = not reported in the original paper).

2D material/system	Substrate (fabric/yarn)	Deposition/Assembly	Function	Key metrics (units)	Operating conditions	Durability	Ref
$Ti_3C_2T_x$ MXene–cotton TENG	Cotton fabric	MXene supported/coated electrode; fabric TENG assembly	Triboelectric nanogenerator (TENG)	Flexible, self-powered sensing; detects subtle and large biomechanical motions; gait-phase monitoring	Human motion; ambient	NR	[123]
Graphene-electrode fabric TENG	Woven/knit fabrics	Ultrasonic spray-coated graphene electrodes	Triboelectric nanogenerator (TENG)	Scalable fabric-based TENG; energy harvesting from joint bending and steps; wearable motion sensing	Human motion; ambient	NR	[123]
MoS_2@PVDF hybrid (bar-printed) †	Flexible film (textile-adjacent)	MoS_2 embedded in PVDF; bar-printed; self-poled	Triboelectric nanogenerator (TENG)	Enhanced triboelectric output; integration via lamination/coating onto fabrics	Human motion/light contact; ambient	NR	[130]
h-BN/PVDF nanofibre PENG †	Electrospun PVDF nanofibre mat	Electrospinning of PVDF with h-BN nanosheets	Piezoelectric nanogenerator (PENG)	High-output PENG; garment-mounted patch for pressure/strain sensing	Human motion/pressure; ambient	NR	[131]

Notes:
1. TENG = triboelectric nanogenerator; PENG = piezoelectric nanogenerator. Human-motion operation implies on-body or bench-simulated joint/finger/wrist/step actuation.
2. Electrical/energy outputs are summarised qualitatively, and numerical values are not reported in the manuscript text.
3. Textile-adjacent devices (films/mats) are included as mechanistic comparators with plausible textile embodiments (lamination, adhesive webs, or encapsulated appliqués).

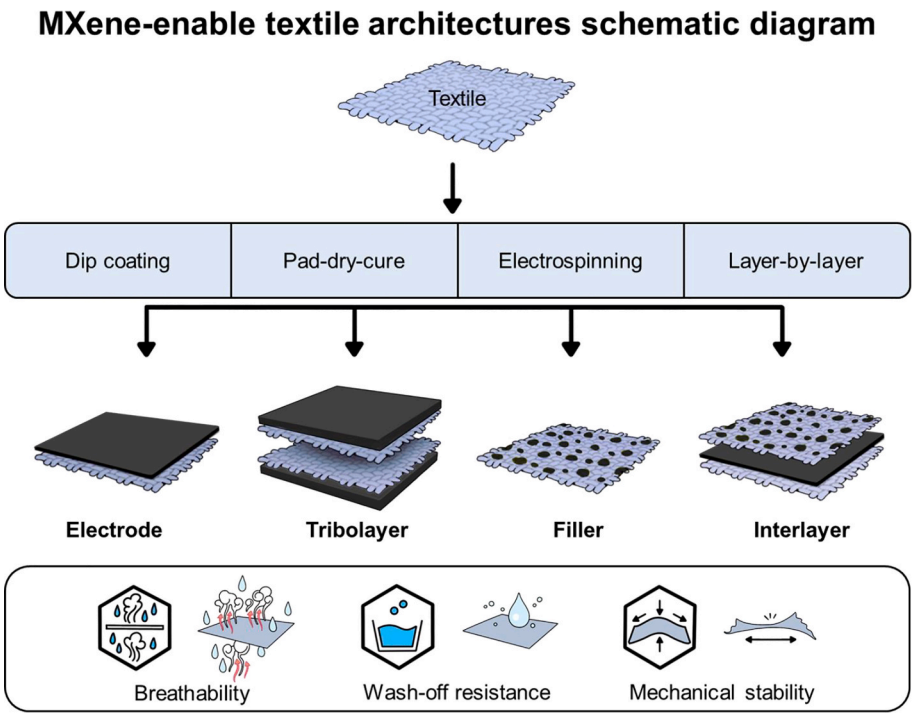

Fig. 17. Schematic of MXene-enabled triboelectric textile architectures. The figure summarises MXene placement options (electrode/tribolayer/filler/interlayer), associated textile-finishing routes, and typical stability constraints relevant to skin-contact wearables (breathability, wash-off, mechanical fatigue) [3,4].

washability review literature underscores the need for harmonised testing beyond ad hoc 'home wash' trials [135].

(v) Manufacturing and system integration. To reach scalable deployment, materials and processes must dovetail with textile production lines (printing, coating, lamination) and support modular, repairable architectures. Direct growth/transfer strategies, as well as 2D heterostructure manufacturing pathways, provide practical guidance for building multilayer stacks with clean interfaces while preserving breathability and drape [28,36].

(vi) Safety, biocompatibility, regulatory translation, and data stewardship. Translation of healthcare e-textiles from laboratory prototypes to clinically credible products requires early alignment with medical-device expectations, because regulatory obligations are driven primarily by intended use, clinical claims, and user population, rather than by the wearable form factor alone. In the European context, devices intended for diagnosis, monitoring, prediction, or treatment fall under the Medical Device Regulation framework (EU MDR 2017/745), whereas in the United States, analogous pathways are governed by FDA device classification and pre-/post-market requirements; consequently, garment-integrated systems are best designed with a "regulatory-by-design" mindset from the outset [136].

For textile finishes that are intended for prolonged skin contact, a structured biological evaluation is required. In practice, this is commonly framed through the ISO 10993 series (risk-based biological evaluation and endpoint selection), with particular emphasis on endpoints relevant to skin-contact wearables (e.g., irritation and sensitisation) and on the assessment of finished, processed devices rather than raw materials [137]. In addition to classical biocompatibility endpoints, 2D-material-enabled textiles warrant explicit consideration of leachables/extractables and particulate release under realistic wear and care conditions. Systematic evidence shows that nanomaterial-treated textiles can release particulate matter during use and washing, and the magnitude and form of release depend strongly on finishing chemistry, mechanical abrasion, and laundering protocol [138,139]. For emerging 2D materials, safety assessment is further complicated by the strong dependence of biological interactions on size, surface chemistry, and transformation/aging, harmonised test protocols and exposure-relevant measurements are therefore central to credible risk evaluation for on-skin applications [140].

Clinical adoption also requires evidence beyond bench characterisation. For wearable diagnostics, validation typically involves comparison against medical-grade reference methods under defined endpoints, with attention to confounders such as motion artefacts, sweat/humidity, and long-duration wear [136]. Although much of the clinical-validation literature concerns non-textile wearables, systematic reviews and meta-analyses illustrate the evidentiary standard expected for diagnostic claims (e.g., pooled sensitivity/specificity against clinical references), underscoring the need for appropriately powered studies and transparent reporting [141]. In the specific case of textile bioelectrodes (e.g., ECG), the stability of the skin–electrode interface (impedance stability and motion artefact susceptibility) should be treated as a first-order translational metric, alongside wash durability and long-term comfort [1].

Finally, because healthcare e-textiles generate sensitive physiological data and increasingly incorporate wireless transmission and embedded analytics, data security, privacy, and integrity constitute essential components of clinical credibility. Surveys and recent analyses of wearable-health monitoring security highlight recurrent vulnerabilities spanning device firmware, wireless links, and data handling; accordingly, secure-by-design architectures (encryption, authentication, secure update mechanisms, and integrity monitoring) should be co-developed with low-power electronics and textile constraints [142] [143].

For clarity, Table 10 summarises a 2D-material-specific translation checklist that links finishing and process options to interface stability, durability, and exposure-related considerations for healthcare textiles.

In summary, maturing synthesis, passivation, and chemical modification, coupled with standardised durability testing and manufacturing-aware integration, position 2D materials as modular building blocks for multifunctional, wash-durable healthcare textiles that integrate sensing, actuation, energy harvesting, and secure data handling [3,35]. Coordinated efforts among materials chemists, textile engineers, and

Table 10
2D-material-specific translation checklist for healthcare textile finishing.

2D-material translation aspect (textile finishing)	What should be defined/reported	Why does it matter?	Evidence/metrics expected	Ref.
Ink/coating processability and formulation stability	Nanosheet type (e.g., GO/rGO, $Ti_3C_2T_x$), lateral size/thickness where available, solvent system, dispersant/binder, solids loading, rheology (for printing), add-on	Determines coatability/printability, network formation on fibres, and reproducibility of electrical/functional response	Viscosity window for printing; add-on mass (mg cm^{-2}); uniformity mapping; batch-to-batch variance	[3,4]
Fibre–2D interfacial chemistry and adhesion	Fibre type (cellulosic/polyamide/polyester), pre-treatments, binder/crosslinker chemistry, encapsulation/topcoat, peel/abrasion tests	Many failures are interfacial (delamination/wash-off) rather than intrinsic; adhesion controls durability and signal drift	Adhesion/abrasion tests; resistance retention after bending/abrasion; microscopy of coating continuity	[1,3]
Percolation network integrity under deformation (fatigue)	Working strain range, cyclic protocol, mechanical mode (bend/stretch/twist), network design (porous/cracked/hierarchical)	2D networks are sensitive to crack growth and network rearrangement; fatigue drives drift/hysteresis	$\Delta R/R$ drift vs cycles; hysteresis; baseline recovery; failure-mode description	[1,3]
Laundering durability and degradation mechanism	Wash protocol (programme, detergent, cycles), drying method, encapsulation strategy; identify degradation pathway (wash-off vs oxidation vs cracking)	"Washable" claims are non-comparable without protocols; 2D coatings can lose conductivity by wash-off or chemical change	Resistance/signal retention after N washes; mass loss/add-on loss; microscopy pre/post wash	[1,3]
Environmental stability (humidity/sweat/oxygen) and transformation	Humidity/sweat exposure protocol, oxidation/passivation strategy (esp. MXenes, BP), termination chemistry where relevant	Several 2D families show performance drift via oxidation/hydration; stability is decisive for on-body wear	Retained conductivity/sensitivity after humidity/sweat aging; chemical signatures of transformation; time-to-failure	[4,37]
Dermal exposure relevance: Leachables/extractables and particulate release from 2D finishes	Release during wear/care (abrasion, flexing, washing), extractables, particle/fragment form (when available), dependence on binder/encapsulation	Clinical adoption for skin-contact textiles requires explicit control of release; finishing chemistry governs exposure	Release quantification under realistic wear/wash; correlation to finishing architecture	[138,139]
2D-material safety is surface-chemistry dependent (size/functionalisation/aging)	Surface chemistry/terminations, size distribution, aging/oxidation state; relevance of testing pristine powder vs immobilised textile coating	Biological interactions depend strongly on surface chemistry and transformations; risk cannot be inferred from "2D" label alone	Exposure-relevant characterisation; transformation-aware safety logic; harmonised reporting of key descriptors	[140]
Skin–electrode interface stability as a 2D-coating design output (ECG/EMG/EEG)	Electrode architecture (coating vs printed), surface roughness/porosity, moisture management, encapsulation at the interface	For textile bioelectrodes, interface stability (motion artefacts, contact stability) depends on coating architecture and finishing	Skin–electrode impedance stability; motion artefact assessment; wear-time stability	[1]
Family-specific constraints: Graphene/GO/rGO	Oxidation state (GO vs rGO), reduction strategy if any, binder/encapsulation choice	Trade-off between processability/adhesion (GO) and conductivity (rGO/graphene); network robustness vs sensitivity tuning	Conductivity vs stability; wash/fatigue retention; reporting of oxidation state	[3]
Family-specific constraints: MXenes (e.g., $Ti_3C_2T_x$)	Termination chemistry (Tx), oxidation mitigation/passivation, humidity sensitivity management	High conductivity and aqueous processability, but environmental instability can dominate unless protected	Conductivity drift under humidity/sweat; retention after washing with protective layers	[3,4]
Family-specific constraints: TMDs and BP	Need for hybridisation for conductivity (TMDs), encapsulation for ambient stability (BP), defect/phase effects only insofar as they affect coatings	Semiconducting behaviour can add functionality but often requires interface engineering; BP is particularly sensitive to ambient degradation	Retention under ambient/sweat; hybrid network stability; practical coating strategies	[3,37]
Family-specific constraints: h-BN and carbon nitrides	Role definition (dielectric/barrier/interlayer; photo/antimicrobial concept), immobilisation to prevent release	Often used as barriers/interlayers or functional additives; translation requires stable immobilisation and comfort-preserving architectures	Layer integrity after washing/fatigue; release control in finished textiles	[3,31]

biomedical researchers will be decisive in translating prototype garments into clinically validated, commercially viable solutions.

6. Conclusions

Two-dimensional (2D) materials have advanced healthcare textiles from proof-of-concept devices to credible, application-oriented platforms. Across graphene and its derivatives, MXenes, TMDs, h-BN, and carbon nitrides, the combination of high surface area, tunable interfacial chemistry, and mechanical compliance has enabled finishes and coatings that preserve fabric handle and breathability while delivering robust electrical, thermal, and photonic functionality. As outlined throughout this review, scalable textile processes, such as pad-dry-cure, dip-coating, printing, electrospinning, and lamination, now support a wide range of functional options. These include strain/pressure and ECG sensing; respiration and humidity monitoring; body temperature readout with localized thermotherapy; self-powered operation through tribo-, piezo-, or thermoelectric conversion; and light-mediated functions ranging from photothermal disinfection to emissivity control.

The field's maturity is clear in its wash-durable performance, low-voltage operation, and the integration of multiple functions (e.g., heating plus sensing or harvesting plus sensing) within a single fabric design. Equally important, chemistry-centric levers, surface terminations, defect engineering, doping/intercalation, and tailored binders have emerged as the bridge between material physics and textile-level reliability, anchoring coatings to fibres, stabilising colloids/inks, and managing environmental reactivity.

At the same time, translation to clinical and everyday use will depend on solving a defined set of challenges: (i) reproducible, large-area synthesis and transfer with atomic-level control of phase, thermal composition, and defects; (ii) environmental privacy, stability, and benign encapsulation compatible with skin contact and laundering; (iii) traceable metrology that links nanoscale chemistry to device drift, hysteresis, and noise; (iv) roll-to-roll, standards-aligned manufacturing and test protocols (including realistic laundry, sweat, abrasion, and flex fatigue); and (v) an end-to-end system design that integrates low-power electronics, secure wireless links, and data privacy with biocompatible materials and safe thermal/electrical operating windows.

Looking forward, the most immediate opportunities lie in applications where textiles' intrinsic advantages, such as comfort, coverage, and continuous wear, are decisive: long-term cardiorespiratory monitoring, rehabilitation feedback, thermal therapy with closed-loop control, and

infection-control garments with on-demand photothermal disinfection. Mid-term, modular 'stacked' finishes (e.g., sensing, actuation, and energy harvesting) and voltage-programmable photonic/thermal responses can produce self-adaptive garments that personalise function to the wearer and context. Real-world deployment will benefit from converging progress in three areas: (i) chemistry and inks that remain stable through storage and laundering; (ii) textile manufacturing routes that preserve drape while ensuring uniform coverage and inter-yarn percolation; and (iii) clinical validation with standardised endpoints, comparing textile readouts against medical-grade references over months of wear.

In summary, 2D materials have transformed textiles into platforms that not only 'carry' sensors but also embody them, integrating sensing, actuation, and energy functions within the fibre architecture itself. With ongoing advances in surface chemistry, scalable processing, durability standards, and human-centered design, 2D-enabled e-textiles are well-positioned to move from laboratory demonstrations to clinically credible, wash-durable, and manufacturable systems for preventive, diagnostic, and therapeutic healthcare.

Founding source

This research did not receive any specific grant from funding agencies in the public, commercial, or not-for-profit sectors.

CRediT authorship contribution statement

Rim Ben Debabis: Writing – original draft, Visualization, Formal analysis. **Agnese D'Agostino:** Visualization, Validation, Formal analysis. **Mariam Hadhri:** Visualization, Validation, Formal analysis. **Veronica Migani:** Writing – original draft, Validation, Methodology, Formal analysis. **Raphael Palucci Rosa:** Visualization, Validation, Formal analysis. **Giuseppe Rosace:** Writing – review & editing, Validation, Supervision, Methodology, Formal analysis, Conceptualization. **Valentina Trovato:** Writing – review & editing, Validation, Supervision, Methodology, Formal analysis, Conceptualization.

Declaration of competing interest

The author declares that they have no known competing financial interests or personal relationships that could have appeared to influence the work reported in this paper.

Acknowledgements

The authors would like to thank Mr. Erico Lima Teodorak Vieira for helping with the design of Figures 1, 15, 16 and 17.

Data availability

Review article

References

[1] S. Zaman, X. Tao, C. Cochrane, V. Koncar, Smart E-textile systems: a review for healthcare applications, Electronics (Basel) 11 (2021) 99, https://doi.org/10.3390/electronics11010099.
[2] C. Cochrane, C. Hertleer, A. Schwarz-Pfeiffer, Smart textiles in health, in: Smart Textiles and Their Applications, Elsevier, 2016: pp. 9–32. Doi: https://doi.org/10.1016/B978-0-08-100574-3.00002-3.
[3] M.M. Atta, Q. Zhang, Recent advances in 2D materials for smart textiles, FlatChem 42 (2023) 100562, https://doi.org/10.1016/j.flatc.2023.100562.
[4] A. Ahmed, M.M. Hossain, B. Adak, S. Mukhopadhyay, Recent advances in 2D MXene integrated smart-textile interfaces for multifunctional applications, Chem. Mater. 32 (2020) 10296–10320, https://doi.org/10.1021/acs.chemmater.0c03392.
[5] M. Stoppa, A. Chiolerio, Wearable electronics and smart textiles: a critical review, Sensors 14 (2014) 11957–11992, https://doi.org/10.3390/s140711957.
[6] I.O. for Standardization, ISO/TR 23383:2020 - Textiles and textile products — Smart (Intelligent) textiles — Definitions, categorisation, applications and standardization needs, (2020).
[7] S. de Mulatier, M. Nasreldin, R. Delattre, M. Ramuz, T. Djenizian, Electronic circuits integration in textiles for data processing in wearable technologies, Adv. Mater. Technol. 3 (2018), https://doi.org/10.1002/admt.201700320.
[8] R. Nayak, L. Wang, R. Padhye, Electronic Textiles for Military Personnel, Electronic Textiles, Elsevier, in, 2015, pp. 239–256, https://doi.org/10.1016/B978-0-08-100201-8.00012-6.
[9] T. Fernández-Caramés, P. Fraga-Lamas, Towards the internet-of-smart-clothing: a review on IoT wearables and garments for creating intelligent connected E-textiles, Electronics (Basel). 7 (2018) 405, https://doi.org/10.3390/electronics7120405.
[10] J. Hu, H. Meng, G. Li, S.I. Ibekwe, A review of stimuli-responsive polymers for smart textile applications, Smart Mater. Struct. 21 (2012) 053001, https://doi.org/10.1088/0964-1726/21/5/053001.
[11] C. Simon, E. Potter, M. McCabe, C. Baggerman, Smart Fabrics Technology Development (2010). Patent number: JSC-Cn-22058.
[12] D. Gupta, Functional clothing - definition and classification, Indian J. Fibre Text. Res. 36 (2011) 321–326.
[13] J.S. Meena, S. Bin Choi, S.-B. Jung, J.-W. Kim, Electronic textiles: new age of wearable technology for healthcare and fitness solutions, Mater. Today Bio 19 (2023) 100565, https://doi.org/10.1016/j.mtbio.2023.100565.
[14] MarketsandMarkets, Pulse Oximeter Market – Global Forecast to 2032, (2025).
[15] Emglare, Emglare Sport T-Shirt, (2025).
[16] S. Afroj, S. Tan, A.M. Abdelkader, K.S. Novoselov, N. Karim, Highly conductive, scalable, and machine washable graphene-based E-textiles for multifunctional wearable electronic applications, Adv. Funct. Mater. 30 (2020), https://doi.org/10.1002/adfm.202000293.
[17] L. Jug, S. Hribernik, A. Ojstršek, Synergic effect of large MXene nanosheets and protective coatings on improved electroconductivity and wash durability of MXene/polymer-modified cotton fabric, Prog. Org. Coat. 200 (2025) 109062, https://doi.org/10.1016/j.porgcoat.2025.109062.
[18] V.T. Novi, A. Gonzalez, J. Brockgreitens, A. Abbas, Highly efficient and durable antimicrobial nanocomposite textiles, Sci. Rep. 12 (2022) 17332, https://doi.org/10.1038/s41598-022-22370-2.
[19] H.R. Hong, J. Kim, C.H. Park, Facile fabrication of multifunctional fabrics: use of copper and silver nanoparticles for antibacterial, superhydrophobic, conductive fabrics, RSC Adv. 8 (2018) 41782–41794, https://doi.org/10.1039/C8RA08310J.
[20] T.I. Shaheen, Nanotechnology for modern textiles: highlights on smart applications, The Journal of The Textile Institute 113 (2022) 2274–2284, https://doi.org/10.1080/00405000.2021.1962625.
[21] B. Gutarowska, E. Matyjas-Zgondek, P. Kulpiński, M. Mroczyńska-Florczak, E. Rutkowski, Long-lasting photocatalytic and antimicrobial activity of cotton towels modified with TiO2 and ZnO nanoparticles, Catalysts 11 (2021) 952, https://doi.org/10.3390/catal11080952.
[22] F. Alhashmi Alamer, K. Althagafy, O. Alsalmi, A. Aldeih, H. Alotaiby, M. Althebaiti, H. Alghamdi, N. Alotibi, A. Saeedi, Y. Zabarmawi, M. Hawsawi, M.A. Alnefaie, Review on PEDOT:PSS-Based Conductive Fabric, ACS Omega 7 (2022) 35371–35386. Doi: https://doi.org/10.1021/acsomega.2c01834.
[23] A.I.J. Alqaderi, N. Ramakrishnan, Carbon-based flexible strain sensors: recent advances and performance insights in human motion detection, Chem. Eng. J. 513 (2025) 162609, https://doi.org/10.1016/j.cej.2025.162609.
[24] K. Zhang, Z. Yang, X. Mao, X.-L. Chen, H.-H. Li, Y.-Y. Wang, Multifunctional textiles/metal−organic frameworks composites for efficient ultraviolet radiation blocking and noise reduction, ACS Appl. Mater. Interfaces 12 (2020) 55316–55323, https://doi.org/10.1021/acsami.0c18147.
[25] M.R. Yazdani McCord, H. Baniasadi, Advancements in form-stabilized phase change materials: stabilization mechanisms, multifunctionalities, and applications—a comprehensive review, mater. Today, Energy 41 (2024) 101532, https://doi.org/10.1016/j.mtener.2024.101532.
[26] M.K. Yapici, T. Alkhidir, Y.A. Samad, K. Liao, Graphene-clad textile electrodes for electrocardiogram monitoring, Sens. Actuators B Chem. 221 (2015) 1469–1474, https://doi.org/10.1016/j.snb.2015.07.111.
[27] X. Xu, M. Luo, P. He, X. Guo, J. Yang, Screen printed graphene electrodes on textile for wearable electrocardiogram monitoring, Appl. Phys. A 125 (2019) 714, https://doi.org/10.1007/s00339-019-3006-x.
[28] A. McCreary, O. Kazakova, D. Jariwala, Z.Y. Al Balushi, An outlook into the flat land of 2D materials beyond graphene: synthesis, properties and device applications, 2D Mater. 8 (2021) 013001. Doi: https://doi.org/10.1088/2053-1583/abc13d.
[29] V. Georgakilas, J.N. Tiwari, K.C. Kemp, J.A. Perman, A.B. Bourlinos, K.S. Kim, R. Zboril, Noncovalent functionalization of graphene and graphene oxide for energy materials, biosensing, catalytic, and biomedical applications, Chem. Rev. 116 (2016) 5464–5519, https://doi.org/10.1021/acs.chemrev.5b00620.
[30] A. Criado, M. Melchionna, S. Marchesan, M. Prato, The covalent functionalization of graphene on substrates, Angew. Chem. Int. Ed. 54 (2015) 10734–10750, https://doi.org/10.1002/anie.201501473.
[31] X. Wang, L. Meng, B. Li, Y. Gong, Heteroatoms/molecules to tune the properties of 2D materials, Mater. Today 47 (2021) 108–130, https://doi.org/10.1016/j.mattod.2020.12.019.
[32] M. Donarelli, L. Ottaviano, 2D materials for gas sensing applications: a review on graphene oxide, MoS2, WS2 and phosphorene, Sensors 18 (2018) 3638, https://doi.org/10.3390/s18113638.

[33] S. Ponnada, S. Naskar, Advanced two-dimensional material-based heterostructures in sustainable energy storage devices, CRC press, Boca Raton (2024), https://doi.org/10.1201/9781003404729.
[34] A. Palariya, S. Ponnada, Introduction and characterization of two-dimensional materials, in: Advanced Two-Dimensional Material-Based Heterostructures in Sustainable Energy Storage Devices, CRC Press, Boca Raton, 2024, pp. 1–15, https://doi.org/10.1201/9781003404729-1.
[35] Y.-C. Lin, R. Torsi, R. Younas, C.L. Hinkle, A.F. Rigosi, H.M. Hill, K. Zhang, S. Huang, C.E. Shuck, C. Chen, Y.-H. Lin, D. Maldonado-Lopez, J.L. Mendoza-Cortes, J. Ferrier, S. Kar, N. Nayir, S. Rajabpour, A.C.T. van Duin, X. Liu, D. Jariwala, J. Jiang, J. Shi, W. Mortelmans, R. Jaramillo, J.M.J. Lopes, R. Engel-Herbert, A. Trofe, T. Ignatova, S.H. Lee, Z. Mao, L. Damian, Y. Wang, M.A. Steves, K.L. Knappenberger, Z. Wang, S. Law, G. Bepete, D. Zhou, J.-X. Lin, M. S. Scheurer, J. Li, P. Wang, G. Yu, S. Wu, D. Akinwande, J.M. Redwing, M. Terrones, J.A. Robinson, Recent advances in 2D material theory, synthesis, properties, and applications, ACS Nano 17 (2023) 9694–9747, https://doi.org/10.1021/acsnano.2c12759.
[36] P.V. Pham, S.C. Bodepudi, K. Shehzad, Y. Liu, Y. Xu, B. Yu, X. Duan, 2D heterostructures for ubiquitous electronics and optoelectronics: principles, opportunities, and challenges, Chem. Rev. 122 (2022) 6514–6613, https://doi.org/10.1021/acs.chemrev.1c00735.
[37] C.R. Ryder, J.D. Wood, S.A. Wells, M.C. Hersam, Chemically tailoring semiconducting two-dimensional transition metal dichalcogenides and black phosphorus, ACS Nano 10 (2016) 3900–3917, https://doi.org/10.1021/acsnano.6b01091.
[38] A. Chaves, J.G. Azadani, H. Alsalman, D.R. da Costa, R. Frisenda, A.J. Chaves, S. H. Song, Y.D. Kim, D. He, J. Zhou, A. Castellanos-Gomez, F.M. Peeters, Z. Liu, C. L. Hinkle, S.-H. Oh, P.D. Ye, S.J. Koester, Y.H. Lee, Ph. Avouris, X. Wang, T. Low, Bandgap engineering of two-dimensional semiconductor materials, NPJ 2D mater, Appl 4 (2020) 29, https://doi.org/10.1038/s41699-020-00162-4.
[39] B. Anasori, Y. Gogotsi (Eds.), 2D Metal Carbides and Nitrides (MXenes), Springer International Publishing, Cham, 2019, https://doi.org/10.1007/978-3-030-19026-2.
[40] W.-J. Ong, L.-L. Tan, Y.H. Ng, S.-T. Yong, S.-P. Chai, Graphitic Carbon Nitride (g-C 3 N 4)-Based Photocatalysts for Artificial Photosynthesis and Environmental Remediation: Are We a Step Closer To Achieving Sustainability?, Chem. Rev. 116 (2016) 7159–7329. Doi: https://doi.org/10.1021/acs.chemrev.6b00075.
[41] P. Moradifar, Y. Liu, J. Shi, M.L. Siukola Thurston, H. Utzat, T.B. van Driel, A. M. Lindenberg, J.A. Dionne, Accelerating quantum materials development with advances in transmission electron microscopy, Chem. Rev. 123 (2023) 12757–12794, https://doi.org/10.1021/acs.chemrev.2c00917.
[42] A. Brown, S. Rundqvist, Refinement of the crystal structure of black phosphorus, Acta Crystallogr. 19 (1965) 684–685, https://doi.org/10.1107/S0365110X65004140.
[43] S. Wu, K.S. Hui, K.N. Hui, 2D black phosphorus: from preparation to applications for electrochemical energy storage, Adv. Sci. 5 (2018), https://doi.org/10.1002/advs.201700491.
[44] J. Qiao, X. Kong, Z.-X. Hu, F. Yang, W. Ji, High-mobility transport anisotropy and linear dichroism in few-layer black phosphorus, Nat. Commun. 5 (2014) 4475, https://doi.org/10.1038/ncomms5475.
[45] J. Tao, W. Shen, S. Wu, L. Liu, Z. Feng, C. Wang, C. Hu, P. Yao, H. Zhang, W. Pang, X. Duan, J. Liu, C. Zhou, D. Zhang, Mechanical and electrical anisotropy of few-layer black phosphorus, ACS Nano 9 (2015) 11362–11370, https://doi.org/10.1021/acsnano.5b05151.
[46] S. Narita, Y. Akahama, Y. Tsukiyama, K. Muro, S. Mori, S. Endo, M. Taniguchi, M. Seki, S. Suga, A. Mikuni, H. Kanzaki, Electrical and optical properties of black phosphorus single crystals, Physica B+C 117–118 (1983) 422–424, https://doi.org/10.1016/0378-4363(83)90547-8.
[47] B.D. Assresahegn, T. Brousse, D. Bélanger, Advances on the use of diazonium chemistry for functionalization of materials used in energy storage systems, Carbon N. Y. 92 (2015) 362–381, https://doi.org/10.1016/j.carbon.2015.05.030.
[48] N. Rabiee, M. Rabiee, Molecular engineering of non-covalent interactions for controlled nanomaterial assembly: chemical principles and materials design, Coord. Chem. Rev. 545 (2025) 217005, https://doi.org/10.1016/j.ccr.2025.217005.
[49] W. Li, Z. Yin, L. Qi, B. Yu, W. Xing, Scalable production of bioinspired MXene/black phosphorene nanocoatings for hydrophobic and fire-safe textiles with tunable electromagnetic interference and exceeding thermal management, Chem. Eng. J. 460 (2023) 141870, https://doi.org/10.1016/j.cej.2023.141870.
[50] Y.-W. Wang, L. Chen, M. Liang, H. Xu, S. Tang, H.-H. Yang, H. Song, Sensitive fluorescence immunoassay of alpha-fetoprotein through copper ions modulated growth of quantum dots in-situ, Sens. Actuators B Chem. 247 (2017) 408–413, https://doi.org/10.1016/j.snb.2017.03.036.
[51] S. Tajik, Z. Dourandish, F. Garkani Nejad, H. Beitollahi, P.M. Jahani, A. Di Bartolomeo, Transition metal dichalcogenides: synthesis and use in the development of electrochemical sensors and biosensors, Biosens. Bioelectron. 216 (2022) 114674, https://doi.org/10.1016/j.bios.2022.114674.
[52] J. Liu, H. Zhang, R. Sun, Y. Liu, Z. Liu, A. Zhou, Z. Yu, Hydrophobic, flexible, and lightweight MXene foams for high-performance electromagnetic-interference shielding, Adv. Mater. 29 (2017), https://doi.org/10.1002/adma.201702367.
[53] R.G. Dickinson, L. Pauling, The CRYSTAL structure of MOLYBDENITE, J. Am. Chem. Soc. 45 (1923) 1466–1471, https://doi.org/10.1021/ja01659a020.
[54] J. Hu, M. Dong, Recent advances in two-dimensional nanomaterials for sustainable wearable electronic devices, J. Nanobiotechnology 22 (2024) 63, https://doi.org/10.1186/s12951-023-02274-7.
[55] N. Kumar, H. Singh, M. Khatri, N. Bhardwaj, 2D-Transition Metal Carbides and Nitrides: Materials for the Next Generation, in: N. Kumar, H. Singh, M. Khatri, N. B.T.-A. of Mx. Bhardwaj Volume 1: Fundamentals and Artificial Intelligence: Machine Learning Interventions (Eds.), American Chemical Society, Washington, DC, 2023: pp. 1–25. Doi: https://doi.org/10.1021/bk-2023-1442.ch001.
[56] S. Zhou, Y. Guan, L. Tan, X. Li, H. Zhu, Q. Zhang, Z. Dong, N. Yang, Y. Cong, Recent advances in multiple transition metal MXenes: synthesis, properties, and applications in energy storage, J. Energy Storage 120 (2025) 116419, https://doi.org/10.1016/j.est.2025.116419.
[57] Z. Lin, H. Shao, K. Xu, P.-L. Taberna, P. Simon, MXenes as high-rate electrodes for energy storage, Trends Chem. 2 (2020) 654–664, https://doi.org/10.1016/j.trechm.2020.04.010.
[58] P. Urbankowski, B. Anasori, T. Makaryan, D. Er, S. Kota, P.L. Walsh, M. Zhao, V. B. Shenoy, M.W. Barsoum, Y. Gogotsi, Synthesis of two-dimensional titanium nitride ti 4 n 3 (MXene), Nanoscale 8 (2016) 11385–11391, https://doi.org/10.1039/C6NR02253G.
[59] B. Yu, D. Chen, Z. Wang, F. Qi, X. Zhang, X. Wang, Y. Hu, B. Wang, W. Zhang, Y. Chen, J. He, W. He, Mo2C quantum dots@graphene functionalized separator toward high-current-density lithium metal anodes for ultrastable Li-S batteries, Chem. Eng. J. 399 (2020) 125837, https://doi.org/10.1016/j.cej.2020.125837.
[60] K. Zhang, J. Sun, J. Song, C. Gao, Z. Wang, C. Song, Y. Wu, Y. Liu, Self-healing ti 3 c 2 MXene/PDMS supramolecular elastomers based on small biomolecules modification for wearable sensors, ACS Appl. Mater. Interfaces 12 (2020) 45306–45314, https://doi.org/10.1021/acsami.0c13653.
[61] A. Ren, J. Zou, H. Lai, Y. Huang, L. Yuan, H. Xu, K. Shen, H. Wang, S. Wei, Y. Wang, X. Hao, J. Zhang, D. Zhao, J. Wu, Z. Wang, Direct laser-patterned MXene–perovskite image sensor arrays for visible-near infrared photodetection, Mater. Horiz. 7 (2020) 1901–1911, https://doi.org/10.1039/D0MH00537A.
[62] M. Chao, Y. Wang, D. Ma, X. Wu, W. Zhang, L. Zhang, P. Wan, Wearable MXene nanocomposites-based strain sensor with tile-like stacked hierarchical microstructure for broad-range ultrasensitive sensing, Nano Energy 78 (2020) 105187, https://doi.org/10.1016/j.nanoen.2020.105187.
[63] Y. Li, X. Zhang, Electrically conductive, optically responsive, and highly orientated ti 3 c 2 t x MXene aerogel fibers, Adv. Funct. Mater. 32 (2022), https://doi.org/10.1002/adfm.202107767.
[64] J. Wang, F. Ma, M. Sun, Graphene, hexagonal boron nitride, and their heterostructures: properties and applications, RSC Adv. 7 (2017) 16801–16822, https://doi.org/10.1039/C7RA00260B.
[65] M.H. Khan, H.K. Liu, X. Sun, Y. Yamauchi, Y. Bando, D. Golberg, Z. Huang, Few-atomic-layered hexagonal boron nitride: CVD growth, characterization, and applications, Mater. Today 20 (2017) 611–628, https://doi.org/10.1016/j.mattod.2017.04.027.
[66] F.A.L. de Souza, G. Sivaraman, J. Hertkorn, R.G. Amorim, M. Fyta, W.L. Scopel, Hybrid 2D nanodevices (graphene/h-BN): selecting NO x gas through the device interface, J. Mater. Chem. A Mater. 7 (2019) 8905–8911, https://doi.org/10.1039/C9TA00674E.
[67] G. Liu, Y. Tang, A.M. Soomro, P. Shen, S. Lu, Y. Cai, H. Wang, Q. Yang, H. Chen, Y. Shi, C. Lin, F. Xu, F. Xu, Z. Wu, X. Chen, D. Cai, J. Kang, Vertically aligned ZnO nanoarray directly orientated on cu paper by h-BN monolayer for flexible and transparent piezoelectric nanogenerator, Nano Energy 109 (2023) 108265, https://doi.org/10.1016/j.nanoen.2023.108265.
[68] W. Zhao, Z. Yan, L. Qian, Graphitic carbon nitride: preparation, properties and applications in energy storage, Engineered Science (2020), https://doi.org/10.30919/es8d1008.
[69] M. Kawaguchi, S. Yagi, H. Enomoto, Chemical preparation and characterization of nitrogen-rich carbon nitride powders, Carbon N. Y. 42 (2004) 345–350, https://doi.org/10.1016/j.carbon.2003.11.004.
[70] E. Kroke, Novel group 14 nitrides, Coord. Chem. Rev. 248 (2004) 493–532, https://doi.org/10.1016/j.ccr.2004.02.001.
[71] M. Ghaemmaghami, R. Mohammadi, Carbon nitride as a new way to facilitate the next generation of carbon-based supercapacitors, sustain, Energy Fuel 3 (2019) 2176–2204, https://doi.org/10.1039/C9SE00313D.
[72] G. Liao, F. He, Q. Li, L. Zhong, R. Zhao, H. Che, H. Gao, B. Fang, Emerging graphitic carbon nitride-based materials for biomedical applications, Prog. Mater. Sci. 112 (2020) 100666, https://doi.org/10.1016/j.pmatsci.2020.100666.
[73] L. Cheng, H. Zhang, X. Li, J. Fan, Q. Xiang, Carbon–Graphitic Carbon Nitride Hybrids for Heterogeneous Photocatalysis, Small 17 (2021). Doi: https://doi.org/10.1002/smll.202005231.
[74] M.S. Nasir, G. Yang, I. Ayub, S. Wang, L. Wang, X. Wang, W. Yan, S. Peng, S. Ramakarishna, Recent development in graphitic carbon nitride based photocatalysis for hydrogen generation, Appl. Catal. B 257 (2019) 117855, https://doi.org/10.1016/j.apcatb.2019.117855.
[75] X. Huo, H. Yi, Y. Fu, Z. An, L. Qin, X. Liu, B. Li, S. Liu, L. Li, M. Zhang, F. Xu, G. Zeng, C. Lai, Porous graphitic carbon nitride nanomaterials for water treatment, environ. Sci, Nano 8 (2021) 1835–1862, https://doi.org/10.1039/D1EN00171J.
[76] J. Sehnert, K. Baerwinkel, J. Senker, Ab initio calculation of solid-state NMR spectra for different triazine and heptazine based structure proposals of g-C 3 n 4, J. Phys. Chem. B 111 (2007) 10671–10680, https://doi.org/10.1021/jp072001k.
[77] S. Verma, R.B.N. Baig, M.N. Nadagouda, R.S. Varma, Selective oxidation of alcohols using photoactive VO@g-C 3 n 4, ACS Sustain. Chem. Eng. 4 (2016) 1094–1098, https://doi.org/10.1021/acssuschemeng.5b01163.
[78] H.-Y. Xu, L.-C. Wu, H. Zhao, L.-G. Jin, S.-Y. Qi, Synergic effect between adsorption and photocatalysis of metal-free g-C3N4 derived from different precursors, PloS One 10 (2015) e0142616, https://doi.org/10.1371/journal.pone.0142616.

[79] Y.-P. Yuan, S.-W. Cao, Y.-S. Liao, L.-S. Yin, C. Xue, Red phosphor/g-C3N4 heterojunction with enhanced photocatalytic activities for solar fuels production, Appl. Catal. B 140–141 (2013) 164–168, https://doi.org/10.1016/j.apcatb.2013.04.006.
[80] S. Bayan, S. Pal, S.K. Ray, Interface engineered silver nanoparticles decorated g-C3N4 nanosheets for textile based triboelectric nanogenerators as wearable power sources, Nano Energy 94 (2022) 106928, https://doi.org/10.1016/j.nanoen.2022.106928.
[81] A. Mohammad, M.A. Zamzami, Construction of carbon cloth modified-Al2O3-g-C3N4 sensor for non-enzymatic electrochemical detection of hydrogen peroxide, Diamond Relat. Mater. 132 (2023) 109600, https://doi.org/10.1016/j.diamond.2022.109600.
[82] L. Bi, Z. Yang, L. Chen, Z. Wu, C. Ye, Compressible AgNWs/Ti 3 c 2 t x MXene aerogel-based highly sensitive piezoresistive pressure sensor as versatile electronic skins, J. Mater. Chem. A Mater. 8 (2020) 20030–20036, https://doi.org/10.1039/D0TA07044K.
[83] W. Wu, L. Wang, Y. Li, F. Zhang, L. Lin, S. Niu, D. Chenet, X. Zhang, Y. Hao, T. F. Heinz, J. Hone, Z.L. Wang, Piezoelectricity of single-atomic-layer MoS2 for energy conversion and piezotronics, Nature 514 (2014) 470–474, https://doi.org/10.1038/nature13792.
[84] C.R. Dean, A.F. Young, I. Meric, C. Lee, L. Wang, S. Sorgenfrei, K. Watanabe, T. Taniguchi, P. Kim, K.L. Shepard, J. Hone, Boron nitride substrates for high-quality graphene electronics, Nat. Nanotechnol. 5 (2010) 722–726, https://doi.org/10.1038/nnano.2010.172.
[85] Y. Zheng, Y. Li, Y. Zhou, K. Dai, G. Zheng, B. Zhang, C. Liu, C. Shen, High-performance wearable strain sensor based on graphene/cotton fabric with high durability and low detection limit, ACS Appl. Mater. Interfaces 12 (2020) 1474–1485, https://doi.org/10.1021/acsami.9b17173.
[86] Y. Zhang, H. Ren, H. Chen, Q. Chen, L. Jin, W. Peng, S. Xin, Y. Bai, Cotton fabrics decorated with conductive graphene nanosheet inks for flexible wearable heaters and strain sensors, ACS Appl. Nano Mater. 4 (2021) 9709–9720, https://doi.org/10.1021/acsanm.1c02076.
[87] D. Wang, D. Li, M. Zhao, Y. Xu, Q. Wei, Multifunctional wearable smart device based on conductive reduced graphene oxide/polyester fabric, Appl. Surf. Sci. 454 (2018) 218–226, https://doi.org/10.1016/j.apsusc.2018.05.127.
[88] S. Chun, W. Son, D.W. Kim, J. Lee, H. Min, H. Jung, D. Kwon, A.-H. Kim, Y.-J. Kim, S.K. Lim, C. Pang, C. Choi, Water-resistant and skin-adhesive wearable electronics using graphene fabric sensor with Octopus-inspired microsuckers, ACS Appl. Mater. Interfaces 11 (2019) 16951–16957, https://doi.org/10.1021/acsami.9b04206.
[89] W. Cao, C. Ma, D. Mao, J. Zhang, M. Ma, F. Chen, MXene-reinforced cellulose nanofibril inks for 3D-printed smart fibres and textiles, Adv. Funct. Mater. 29 (2019), https://doi.org/10.1002/adfm.201905898.
[90] R. Liu, J. Li, M. Li, Q. Zhang, G. Shi, Y. Li, C. Hou, H. Wang, MXene-coated air-permeable pressure-sensing fabric for smart wear, ACS Appl. Mater. Interfaces 12 (2020) 46446–46454, https://doi.org/10.1021/acsami.0c11715.
[91] J. Luo, S. Gao, H. Luo, L. Wang, X. Huang, Z. Guo, X. Lai, L. Lin, R.K.Y. Li, J. Gao, Superhydrophobic and breathable smart MXene-based textile for multifunctional wearable sensing electronics, Chem. Eng. J. 406 (2021) 126898, https://doi.org/10.1016/j.cej.2020.126898.
[92] X. Zheng, J. Shen, Q. Hu, W. Nie, Z. Wang, L. Zou, C. Li, Vapor phase polymerized conducting polymer/MXene textiles for wearable electronics, Nanoscale 13 (2021) 1832–1841, https://doi.org/10.1039/D0NR07433K.
[93] L. Liu, L. Wang, X. Liu, W. Yuan, M. Yuan, Q. Xia, Q. Hu, A. Zhou, High-performance wearable strain sensor based on MXene@cotton fabric with network structure, Nanomaterials 11 (2021) 889, https://doi.org/10.3390/nano11040889.
[94] S. Seyedin, S. Uzun, A. Levitt, B. Anasori, G. Dion, Y. Gogotsi, J.M. Razal, MXene composite and coaxial fibers with high stretchability and conductivity for wearable strain sensing textiles, Adv. Funct. Mater. 30 (2020), https://doi.org/10.1002/adfm.201910504.
[95] X. Zheng, Y. Wang, W. Nie, Z. Wang, Q. Hu, C. Li, P. Wang, W. Wang, Elastic polyaniline nanoarrays/MXene textiles for all-solid-state supercapacitors and anisotropic strain sensors, Compos. Part A Appl. Sci. Manuf. 158 (2022) 106985, https://doi.org/10.1016/j.compositesa.2022.106985.
[96] T. Raza, M.K. Tufail, A. Ali, A. Boakye, X. Qi, Y. Ma, A. Ali, L. Qu, M. Tian, Wearable and flexible multifunctional sensor based on laser-induced graphene for the sports monitoring system, ACS Appl. Mater. Interfaces 14 (2022) 54170–54181, https://doi.org/10.1021/acsami.2c14847.
[97] S. Zhang, J. Xu, PDMS/ag/Mxene/polyurethane conductive yarn as a highly reliable and stretchable strain sensor for human motion monitoring, Polymers (Basel). 14 (2022) 5401, https://doi.org/10.3390/polym14245401.
[98] X. Xu, M. Luo, P. He, J. Yang, Washable and flexible screen printed graphene electrode on textiles for wearable healthcare monitoring, J. Phys. D Appl. Phys. 53 (2020) 125402, https://doi.org/10.1088/1361-6463/ab5f4a.
[99] S.K. Sinha, Y. Noh, N. Reljin, G.M. Treich, S. Hajeb-Mohammadalipour, Y. Guo, K. H. Chon, G.A. Sotzing, Screen-printed PEDOT: PSS electrodes on commercial finished textiles for electrocardiography, ACS Appl. Mater. Interfaces 9 (2017) 37524–37528, https://doi.org/10.1021/acsami.7b09954.
[100] M. Akter Shathi, C. Minzhi, N.A. Khoso, H. Deb, A. Ahmed, W. Sai Sai, All organic graphene oxide and poly (3, 4-ethylene dioxythiophene) - poly (styrene sulfonate) coated knitted textile fabrics for wearable electrocardiography (ECG) monitoring, Synth. Met. 263 (2020) 116329, https://doi.org/10.1016/j.synthmet.2020.116329.
[101] M.A. Shathi, M. Chen, N.A. Khoso, M.T. Rahman, B. Bhattacharjee, Graphene coated textile based highly flexible and washable sports bra for human health monitoring, Mater. Des. 193 (2020) 108792, https://doi.org/10.1016/j.matdes.2020.108792.
[102] M.R. Islam, S. Afroj, C. Beach, M.H. Islam, C. Parraman, A. Abdelkader, A. J. Casson, K.S. Novoselov, N. Karim, Fully printed and multifunctional graphene-based wearable e-textiles for personalized healthcare applications, IScience 25 (2022) 103945, https://doi.org/10.1016/j.isci.2022.103945.
[103] S. Guler, A. Golparvar, O. Ozturk, M.K. Yapici, Ear electrocardiography with soft graphene textiles for hearable applications, IEEE Sens. Lett. 6 (2022) 1–4, https://doi.org/10.1109/LSENS.2022.3198279.
[104] L. Liu, W. Chen, H. Zhang, Q. Wang, F. Guan, Z. Yu, Flexible and multifunctional silk textiles with biomimetic leaf-like MXene/silver nanowire nanostructures for electromagnetic interference shielding, humidity monitoring, and self-derived hydrophobicity, Adv. Funct. Mater. 29 (2019), https://doi.org/10.1002/adfm.201905197.
[105] Y. Wang, L. Zhang, Z. Zhang, P. Sun, H. Chen, High-sensitivity wearable and flexible humidity sensor based on graphene oxide/non-woven fabric for respiration monitoring, Langmuir 36 (2020) 9443–9448, https://doi.org/10.1021/acs.langmuir.0c01315.
[106] L. Xu, H. Zhai, X. Chen, Y. Liu, M. Wang, Z. Liu, M. Umar, C. Ji, Z. Chen, L. Jin, Z. Liu, Q. Song, P. Yue, Y. Li, T.T. Ye, Coolmax/graphene-oxide functionalized textile humidity sensor with ultrafast response for human activities monitoring, Chem. Eng. J. 412 (2021) 128639, https://doi.org/10.1016/j.cej.2021.128639.
[107] X. Zhao, Y. Long, T. Yang, J. Li, H. Zhu, Simultaneous high sensitivity sensing of temperature and humidity with graphene woven fabrics, ACS Appl. Mater. Interfaces 9 (2017) 30171–30176, https://doi.org/10.1021/acsami.7b09184.
[108] S. Choi, H. Yu, J. Jang, M. Kim, S. Kim, H.S. Jeong, I. Kim, Nitrogen-doped single graphene fiber with platinum water dissociation catalyst for wearable humidity sensor, Small 14 (2018), https://doi.org/10.1002/smll.201703934.
[109] Y. Wang, T. Yang, J. Lao, R. Zhang, Y. Zhang, M. Zhu, X. Li, X. Zang, K. Wang, W. Yu, H. Jin, L. Wang, H. Zhu, Ultra-sensitive graphene strain sensor for sound signal acquisition and recognition, Nano Res. 8 (2015) 1627–1636, https://doi.org/10.1007/s12274-014-0652-3.
[110] P. Li, L. Zhao, Z. Jiang, M. Yu, Z. Li, X. Zhou, Y. Zhao, A wearable and sensitive graphene-cotton based pressure sensor for human physiological signals monitoring, Sci. Rep. 9 (2019) 14457, https://doi.org/10.1038/s41598-019-50997-1.
[111] L.-Q. Tao, H. Tian, Y. Liu, Z.-Y. Ju, Y. Pang, Y.-Q. Chen, D.-Y. Wang, X.-G. Tian, J.-C. Yan, N.-Q. Deng, Y. Yang, T.-L. Ren, An intelligent artificial throat with sound-sensing ability based on laser induced graphene, Nat. Commun. 8 (2017) 14579, https://doi.org/10.1038/ncomms14579.
[112] Y. Wei, Y. Qiao, G. Jiang, Y. Wang, F. Wang, M. Li, Y. Zhao, Y. Tian, G. Gou, S. Tan, H. Tian, Y. Yang, T.-L. Ren, A wearable skinlike ultra-sensitive artificial graphene throat, ACS Nano 13 (2019) 8639–8647, https://doi.org/10.1021/acsnano.9b03218.
[113] G. Rajan, J.J. Morgan, C. Murphy, E. Torres Alonso, J. Wade, A.K. Ott, S. Russo, H. Alves, M.F. Craciun, A.I.S. Neves, Low Operating Voltage Carbon–Graphene Hybrid E-textile for Temperature Sensing, ACS Appl. Mater. Interfaces 12 (2020) 29861–29867. Doi: https://doi.org/10.1021/acsami.0c08397.
[114] F. Wang, J. Jiang, F. Sun, L. Sun, T. Wang, Y. Liu, M. Li, Flexible wearable graphene/alginate composite non-woven fabric temperature sensor with high sensitivity and anti-interference, Cellulose 27 (2020) 2369–2380, https://doi.org/10.1007/s10570-019-02951-7.
[115] W. Fan, T. Liu, F. Wu, S. Wang, S. Ge, Y. Li, J. Liu, H. Ye, R. Lei, C. Wang, Q. Che, Y. Li, An antisweat interference and highly sensitive temperature sensor based on poly(3,4-ethylenedioxythiophene)–poly(styrenesulfonate) fiber coated with polyurethane/graphene for real-time monitoring of body temperature, ACS Nano 17 (2023) 21073–21082, https://doi.org/10.1021/acsnano.3c04246.
[116] H. Yuan, H. Zhang, K. Huang, Y. Cheng, K. Wang, S. Cheng, W. Li, J. Jiang, J. Li, C. Tu, X. Wang, Y. Qi, Z. Liu, Dual-emitter graphene glass fiber fabric for radiant heating, ACS Nano 16 (2022) 2577–2584, https://doi.org/10.1021/acsnano.1c09269.
[117] X. Zhao, L.-Y. Wang, C.-Y. Tang, X.-J. Zha, Y. Liu, B.-H. Su, K. Ke, R.-Y. Bao, M.-B. Yang, W. Yang, Smart ti 3 c 2 t x MXene fabric with fast humidity response and joule heating for healthcare and medical therapy applications, ACS Nano 14 (2020) 8793–8805, https://doi.org/10.1021/acsnano.0c03391.
[118] Q. Wang, H. Zhang, J. Liu, S. Zhao, X. Xie, L. Liu, R. Yang, N. Koratkar, Z. Yu, Multifunctional and water-resistant MXene-decorated polyester textiles with outstanding electromagnetic interference shielding and joule heating performances, Adv. Funct. Mater. 29 (2019), https://doi.org/10.1002/adfm.201806819.
[119] X. Zhang, X. Wang, Z. Lei, L. Wang, M. Tian, S. Zhu, H. Xiao, X. Tang, L. Qu, Flexible MXene-decorated fabric with interwoven conductive networks for integrated joule heating, electromagnetic interference shielding, and strain sensing performances, ACS Appl. Mater. Interfaces 12 (2020) 14459–14467, https://doi.org/10.1021/acsami.0c01182.
[120] M.D. Langer, W. Huang, A. Ghanem, Y. Guo, G.K. Lewis, Skin temperature increase mediated by wearable, long duration, low-intensity therapeutic ultrasound, in (2017) 120002, https://doi.org/10.1063/1.4977642.
[121] N.A. Martin, S. Falder, A review of the evidence for threshold of burn injury, Burns 43 (2017) 1624–1639, https://doi.org/10.1016/j.burns.2017.04.003.
[122] J. Fan, M. Yuan, L. Wang, Q. Xia, H. Zheng, A. Zhou, MXene supported by cotton fabric as electrode layer of triboelectric nanogenerators for flexible sensors, Nano Energy 105 (2023) 107973, https://doi.org/10.1016/j.nanoen.2022.107973.
[123] K. Sreeja Sadanandan, Z. Saadi, C. Murphy, I. Grikalaite, M.F. Craciun, A.I. S. Neves, Fabric-based triboelectric nanogenerators with ultrasonic spray coated

graphene electrodes, Nano Energy 116 (2023) 108797, https://doi.org/10.1016/j.nanoen.2023.108797.
[124] N.A. Khoso, X. Jiao, X. GuangYu, S. Tian, J. Wang, Enhanced thermoelectric performance of graphene based nanocomposite coated self-powered wearable e-textiles for energy harvesting from human body heat, RSC Adv. 11 (2021) 16675–16687, https://doi.org/10.1039/D0RA10783B.
[125] Q. Zhang, X. Xiao, G. Wang, X. Ming, X. Liu, H. Wang, H. Yang, W. Xu, X. Wang, Silk-based systems for highly efficient photothermal conversion under one sun: portability, flexibility, and durability, J. Mater. Chem. A Mater. 6 (2018) 17212–17219, https://doi.org/10.1039/C8TA05193C.
[126] P. Kumar, S. Roy, A. Sarkar, A. Jaiswal, Reusable MoS 2 -modified antibacterial fabrics with photothermal disinfection properties for repurposing of personal protective masks, ACS Appl. Mater. Interfaces 13 (2021) 12912–12927, https://doi.org/10.1021/acsami.1c00083.
[127] M.S. Ergoktas, G. Bakan, P. Steiner, C. Bartlam, Y. Malevich, E. Ozden-Yenigun, G. He, N. Karim, P. Cataldi, M.A. Bissett, I.A. Kinloch, K.S. Novoselov, C. Kocabas, Graphene-enabled adaptive infrared textiles, Nano Lett. 20 (2020) 5346–5352, https://doi.org/10.1021/acs.nanolett.0c01694.
[128] L. Zhou, N. Liu, L. Feng, M. Zhao, P. Wu, Y. Chai, J. Liu, P. Zhu, R. Guo, Multifunctional electrospun asymmetric wettable membrane containing black phosphorus/Rg1 for enhancing infected wound healing, Bioeng. Transl. Med. 7 (2022), https://doi.org/10.1002/btm2.10274.
[129] K. Zhu, H. Yao, J. Song, Q. Liao, S. He, T. Guang, H. Wang, X. Hao, B. Lu, T. Lin, H. Cheng, X. Liu, L. Qu, Temperature-adaptive dual-modal photonic textiles for thermal management, Sci. Adv. 10 (2024), https://doi.org/10.1126/sciadv.adr2062.
[130] B. Hedau, B.-C. Kang, T.-J. Ha, Enhanced triboelectric effects of self-poled MoS 2 -embedded PVDF hybrid nanocomposite films for Bar-printed wearable triboelectric nanogenerators, ACS Nano 16 (2022) 18355–18365, https://doi.org/10.1021/acsnano.2c06257.
[131] P. Yadav, T.D. Raju, S. Badhulika, Self-poled hBN-PVDF nanofiber mat-based Low-cost, ultrahigh-performance piezoelectric nanogenerator for biomechanical energy harvesting, ACS Appl. Electron. Mater. 2 (2020) 1970–1980, https://doi.org/10.1021/acsaelm.0c00272.
[132] J. Fan, G. Zhang, J. Yang, A. Zhou, MXenes in triboelectric nanogenerators (TENGs): present status and the future, J. Adv. Ceram. 14 (2025) 9221087, https://doi.org/10.26599/JAC.2025.9221087.
[133] H. Zhu, S. McDonnell, X. Qin, A. Azcatl, L. Cheng, R. Addou, J. Kim, P.D. Ye, R. M. Wallace, Al 2 o 3 on black phosphorus by atomic layer deposition: An in situ interface study, ACS Appl. Mater. Interfaces 7 (2015) 13038–13043, https://doi.org/10.1021/acsami.5b03192.
[134] G. Abellán, S. Wild, V. Lloret, N. Scheuschner, R. Gillen, U. Mundloch, J. Maultzsch, M. Varela, F. Hauke, A. Hirsch, Fundamental insights into the degradation and stabilization of thin layer black phosphorus, J. Am. Chem. Soc. 139 (2017) 10432–10440, https://doi.org/10.1021/jacs.7b04971.
[135] S. Rotzler, M. von Krshiwoblozki, M. Schneider-Ramelow, Washability of e-textiles: current testing practices and the need for standardization, Text. Res. J. 91 (2021) 2401–2417, https://doi.org/10.1177/0040517521996727.
[136] N. Jiang, J.E. Mück, A.K. Yetisen, The regulation of wearable medical devices, Trends Biotechnol. 38 (2020) 129–133, https://doi.org/10.1016/j.tibtech.2019.06.004.
[137] V.I. Sevastianov, N.V. Perova, E.V. Arzumanyants, N.M. Perova, N. V. Kaminskaya, I.A. Dovzhik, Evaluation of the biological effect of medical devices: general requirements for biological safety (analytical review), Inorg. Mater. Appl. Res. 15 (2024) 1300–1310, https://doi.org/10.1134/S2075113324700916.
[138] Z. Beigzadeh, M. Kolahdouzi, S. Kalantary, F. Golbabaei, A systematic review of released nano-particles from commercial nano-textiles during use and washing, J. Ind. Text. 54 (2024), https://doi.org/10.1177/15280837241254512.
[139] P. Limpiteeprakan, S. Babel, J. Lohwacharin, S. Takizawa, Release of silver nanoparticles from fabrics during the course of sequential washing, Environ. Sci. Pollut. Res. 23 (2016) 22810–22818, https://doi.org/10.1007/s11356-016-7486-3.
[140] H. Lin, T. Buerki-Thurnherr, J. Kaur, P. Wick, M. Pelin, A. Tubaro, F.C. Carniel, M. Tretiach, E. Flahaut, D. Iglesias, E. Vázquez, G. Cellot, L. Ballerini, V. Castagnola, F. Benfenati, A. Armirotti, A. Sallustrau, F. Taran, M. Keck, C. Bussy, S. Vranic, K. Kostarelos, M. Connolly, J.M. Navas, F. Mouchet, L. Gauthier, J. Baker, B. Suarez-Merino, T. Kanerva, M. Prato, B. Fadeel, A. Bianco, Environmental and health impacts of graphene and other two-dimensional materials: a graphene flagship perspective, ACS Nano 18 (2024) 6038–6094, https://doi.org/10.1021/acsnano.3c09699.
[141] O. Sibomana, C.M. Hakayuwa, A. Obianke, H. Gahire, J. Munyantore, M. M. Chilala, Diagnostic accuracy of ECG smart chest patches versus PPG smartwatches for atrial fibrillation detection: a systematic review and meta-analysis, BMC Cardiovasc. Disord. 25 (2025) 132, https://doi.org/10.1186/s12872-025-04582-2.
[142] B. Zhang, C. Chen, I. Lee, K. Lee, K.-L. Ong, A survey on security and privacy issues in wearable health monitoring devices, Comput. Secur. 155 (2025) 104453, https://doi.org/10.1016/j.cose.2025.104453.
[143] M. Ulloa-Zamora, C. Barría-Huidobro, M. Sánchez-Rubio, L. Galeazzi, Integral security pillars for medical devices: a comprehensive analysis, Appl. Sci. 15 (2025) 6634, https://doi.org/10.3390/app15126634.